University of California, Merced

Mathematical Modeling and Parameter Estimation Uncovers the Role of TFPI in the Regulation of Factor Xa

A Capstone submitted in partial satisfaction of the requirements for the degree of Master of Science

in

Applied Mathematics

by

AMANDEEP KAUR

Committee in charge:
Professor Suzanne Sindi, Chair
Professor Erica Rutter

2023

This is to certify that I have examined a copy of a capstone project report by

Amandeep Kaur

and found it satisfactory in all respects, and that any and all revisions
required by the examining committee have been made.

Applied Mathematics
Graduate Studies Chair:

Reading Committee:

Committee Chair / Research Advisor:

_____
Professor Maxime Theillard

_____
Professor Erica Rutter

_____
Professor Suzanne Sindi

Date _____

Abstract

Blood coagulation is a series of biochemical reactions necessary to form a blood clot upon a vascular injury. The process occurs in three stages (initiation, amplification, and propagation) and in the presence of flow. To regulate bleeding disorders, the clotting system involves inhibition mechanisms at each stage. Initiation in the tissue factor pathway begins when clotting factor VIIa in the plasma binds its cofactor, tissue factor (TF) forming an active enzyme complex (TF:VIIa). Next, clotting factor X in the plasma binds with TF:VIIa and is enzymatically cleaved into activated factor X (Xa). Xa is required for other reactions as coagulation progresses.

Tissue factor pathway inhibitor (TFPI) is known to be a strong inhibitor during the initiation phase, with the primary mechanism of binding to Xa in the plasma and then rebinding to TF:VIIa to form the quaternary complex TF:VIIa:Xa:TFPI. However, previous mathematical models of TFPI inhibition predict contradicting results. Some studies suggest that TFPI is a powerful inhibitor for Xa inhibition and others claim that it is a weak inhibitor because flow acts as a more potent inhibitor than TFPI.

In this study, I re-investigated the mechanisms of TFPI inhibition by considering a previous static experimental study of TFPI by Baugh et. al [2] where two inhibitory mechanisms were hypothesized to exist. The suggested reaction scheme, which incorporated both an *Indirect Binding* mechanism and a *Direct Binding* mechanism for TFPI inhibition, was never studied by Baugh et. al. [2]. I used a mathematical model based on this scheme and a constrained optimization framework to fit this proposed reaction scheme to multiple sets of data simultaneously. I found that this scheme for TFPI better fits the experimental data, explains the role of TFPI in regulating factor Xa under static conditions, and is consistent with the previously known kinetic rates and rate constants. Next, I studied the two mechanisms in the presence of flow to understand which mechanism can explain the role of TFPI in inhibiting the formation of Xa. I discovered that *Direct Binding* mechanism is essential for Xa inhibition by TFPI in the presence of flow.

Keywords: Mathematical modeling, TFPI, factor X, constrained optimization, parameter estimation.

Contents

1 Introduction to Blood Coagulation and Motivation

Blood coagulation is a complex system of biochemical reactions that are required to form a clot in response to injury (Figure 1(a)). The process is initiated by the exposure of tissue factor and collagen on the surface of subendothelial cells. This exposure triggers the activation and adhesion of zymogens, enzymes, and platelets, leading to thrombin formation. Thrombin then cleaves fibrinogen into fibrin monomers, which polymerize to form a meshwork that stabilizes the clot. Thrombin is one of the most important clotting factors in the coagulation cascade because it is responsible for forming a stable blood clot at the site of injury, which allows the damaged vessel to repair and ultimately leads to the restoration of normal blood flow. However, both bleeding disorders and clotting irregularities can disrupt the coagulation process. For instance, underclotting can be a result of deadly illnesses such as von Willebrand disease and hemophilia [25], while overclotting may lead to fatal diseases such as pulmonary embolism, heart attacks, and strokes [13]. Therefore, it is crucial to understand the underlying dynamics of the clotting process and its regulation to prevent disease complications caused by bleeding disorders and clotting irregularities.

Mathematical modeling has been used to gain insight into this complex process, but many questions still need to be answered including the role of tissue factor pathway inhibitor (TFPI). One role of TFPI is to inhibit the activation of clotting factor X in the initiation phase. As depicted in Figure 1(b), the factor X becomes activated (denoted Xa) by binding with the enzyme complex TF:VIIa, which is fixed at the injury site and is composed of clotting factor VIIa and tissue factor (TF). Xa plays a significant role in the coagulation cascade since it combines with Va to form the complex prothrombinase, which activates prothrombin (factor II) to thrombin (factor IIa). TFPI inhibits the activation of X by targeting TF:VIIa through two distinct mechanisms. *Indirect Binding* (depicted in red) involves the formation of a complex Xa:TFPI in the fluid, which can bind to TF:VIIa, blocking its ability to activate additional X. *Direct Binding* (depicted in blue) operates through TFPI binding directly to Xa that is already bound to TF:VIIa, thereby inhibiting the enzyme activity and ultimately preventing the release of Xa.

Previous mathematical models disagree on the role of TFPI in regulating Xa activation. Some of these models are based on static systems, i.e. describing the experiments in a test tube. For these kinds of systems of TFPI, models and data have suggested that TFPI plays a crucial role in coagulation. For instance, one static study suggested that thrombin generation is sensitive to TFPI [8]. But for models considering coagulation under flow, a study has suggested that flow itself is a more potent inhibitor than TFPI [10]. However, clinical studies conducted on knockout mice have shown that the lack of TFPI Kunitz 1 domain (Xa dependent inhibition of TF:VIIa) leads to embryonic death and claimed that TFPI is necessary for embryogenesis [20, 29].There are several reasons why the role of TFPI is not fully understood. We may not fully understand the biological mechanisms behind TFPI's role, or perhaps

the mathematical model used to describe TFPI is incomplete from a biological standpoint. The conventional mechanism used to understand TFPI may be insufficient in comprehending its full role. Additionally, the kinetic rates used in current models may be incorrect. Therefore, a systematic study is much needed to determine the exact role of TFPI.

To fill the gap in the knowledge, my study focuses on understanding which inhibition mechanism explains the role of TFPI in inhibiting the activation of factor X in the presence of flow. First, I revisit previously reported experimental data in a new way and considered a model including two mechanisms of TFPI inhibition (standard models include only 1). I conduct a thorough mathematical analysis of the model based on the proposed scheme to establish a set of kinetic rates that is consistent with the experimental data. I employ constrained optimization enforcing known values and relationships to fit the previously reported data simultaneously. Because the coagulation process occurs in the presence of flow, I develop and analyze an ODEs flow model to understand how the system behaves when both *Direct Binding* and *Indirect Binding* are at play.

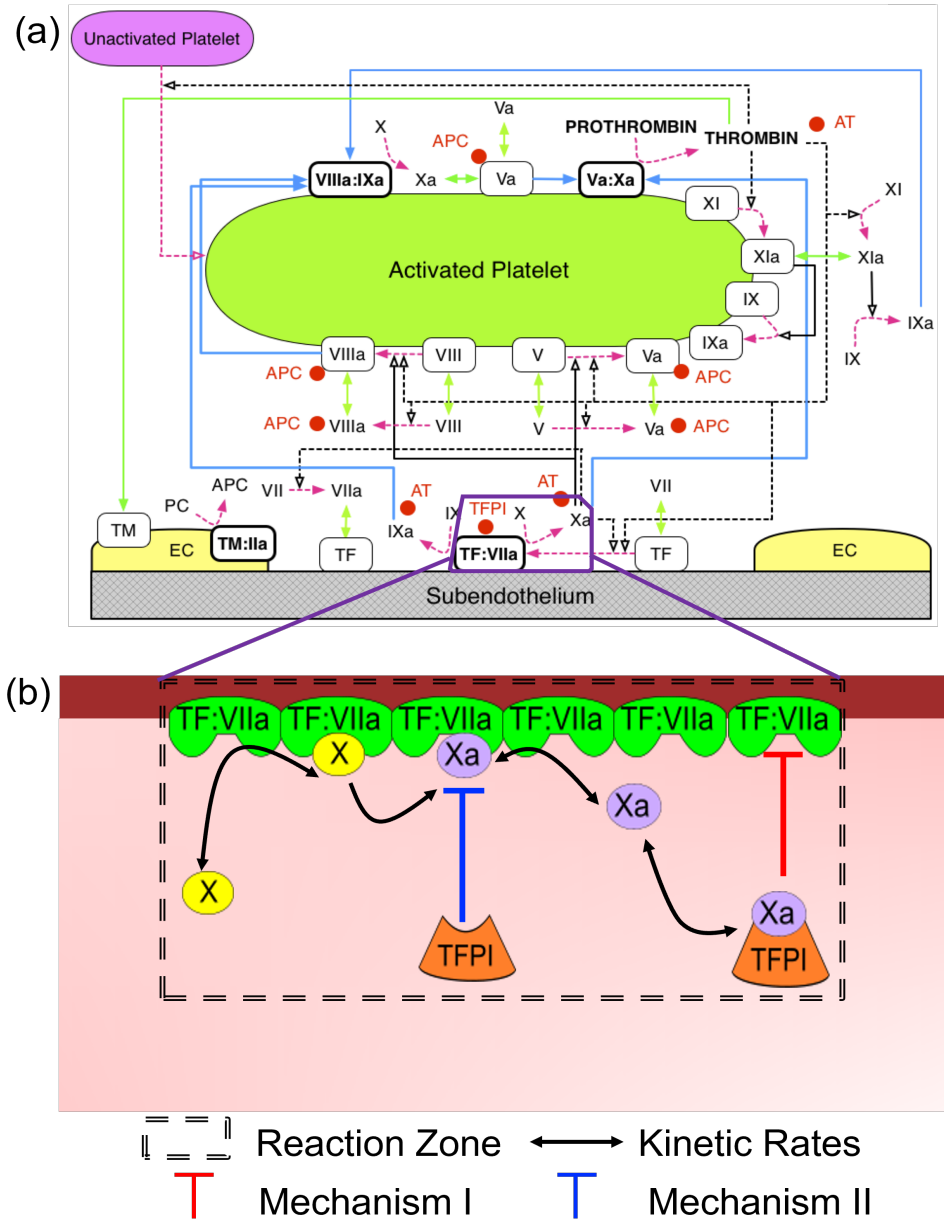

Figure 1: Blood Coagulation Dynamics. (a) Schematic of coagulation cascade [28]. (b) During the initiation process, clotting factor X, present in the plasma, becomes activated factor X (denoted Xa) by binding with TF:VIIa. Double-headed solid black arrows represent binding/unbinding interactions. The single head arrow indicates the catalytic reaction. TFPI inhibits this activation through two biochemical mechanisms: *Indirect Binding* (in red) and *Direct Binding* (in blue).

2 Modeling Inhibition of Factor X Activation by TFPI in the Presence and Absence of Flow

This Chapter focuses on understanding the role of TFPI in regulating factor X activation and TFPI inhibition in the absence and presence of flow. It is divided into four sections. The first Section 2.1 introduces the reader to modeling biochemical reactions in general and develops background knowledge of the published experimental data and previous modeling of Xa activation and TFPI inhibition mechanisms. The second Section 2.2 describes the mathematical model for a closed system (i.e. without the presence of flow) and the constrained optimization method used to discover the precise role of TFPI in inhibiting the formation of factor X. The third Section 2.3 develops the mathematical model to understand how the TFPI inhibition mechanisms behave in the presence of flow. The last Section 2.4 summarizes the major takeaways from my study.

2.1 Modeling Biochemical Reactions, Background on Experimental Data, and Previous Modeling Work

I begin by describing the the modeling of of biochemical reactions in general, the background on experimental data, and then provide details about the evolution of the schemes used to describe the formation of factor Xa and its inhibition by TFPI.

2.1.1 Modeling of Biochemical Reactions

Let's consider the following biochemical reaction

$$A + B \xrightarrow{k_{+i}} A{:}B \tag{R1}$$

where the two reactants A and B can bind together to form the complex $A{:}B$ with the binding rate k_{+i} for a reaction type i. The reactants A, B, and the complex $A{:}B$ are measured in concentrations (e.g., nM). The concentration is denoted as $[\cdot]$; for example, $[A]$ symbolizes the concentration of A. Applying the Law of Mass Action, which states that the instantaneous rate of any reaction at a constant temperature is proportional to the product of the concentrations of each reactant involved in the reaction and the rate coefficient [21], one can express the rate of change in concentration of $A{:}B$ due to reaction (R1) using the following ordinary differential equation (ODE),

$$\frac{d[A{:}B]}{dt} = \underbrace{k_{+i}[A][B]}_{\substack{\text{Binding} \\ \text{of } A \text{ to } B}}. \tag{1}$$

Note that the binding rate k_{+i} is measured in 1/(concentration×time) or 1/([·]×time) as explained below:

$$\frac{d[A{:}B]}{dt} = k_{+i}[A][B]$$
$$\frac{[\cdot]}{\text{time}} = k_{+i}[\cdot][\cdot] = \frac{1}{\cancel{[\cdot]} \times \text{time}}\cancel{[\cdot]}[\cdot] = \frac{[\cdot]}{\text{time}}.$$

When a biochemical reaction is bidirectional, the reaction scheme for A, B, and $A{:}B$ is written as

$$A + B \underset{k_{-i}}{\overset{k_{+i}}{\rightleftharpoons}} A{:}B. \tag{R2}$$

Here, k_{+i} and k_{-i} denote binding and unbinding rates respectively. The unit of k_{-i} is 1/time. Applying the Law of Mass Action, one can derive a system of ordinary differential equations ODEs for the concentrations of all the species from both reactions as follows:

$$\frac{d[A]}{dt} = -\underbrace{k_{+i}[A][B]}_{\substack{\text{Binding} \\ \text{of } A \text{ to } B}} + \underbrace{k_{-i}[A{:}B]}_{\substack{\text{Unbinding} \\ \text{of } A \text{ from } A{:}B}} \tag{2a}$$

$$\frac{d[B]}{dt} = -\underbrace{k_{+i}[A][B]}_{\substack{\text{Binding} \\ \text{of } A \text{ to } B}} + \underbrace{k_{-i}[A{:}B]}_{\substack{\text{Unbinding} \\ \text{of } B \text{ from } A{:}B}} \tag{2b}$$

$$\frac{d[A{:}B]}{dt} = \underbrace{k_{+i}[A][B]}_{\substack{\text{Binding} \\ \text{of } A \text{ to } B}} - \underbrace{k_{-i}[A{:}B]}_{\substack{\text{Unbinding} \\ \text{of } A \text{ from } A{:}B}} . \tag{2c}$$

Now, let $[A_{eq}]$, $[B_{eq}]$, and $[A{:}B_{eq}]$ denote the concentration of A, B, and $A{:}B$ after the reaction has come to an equilibrium (i.e. the concentrations are not changing), then each of the differential equations (2a- 2c) reaches a steady state $\frac{d[\cdot]}{dt} = 0$ which implies mathematically:

$$\frac{k_{-i}}{k_i} = \frac{[A_{eq}][B_{eq}]}{[A{:}B_{eq}]}.$$

Let the equilibrium constant $K_{D,i}$, also known as dissociation constant, be defined as

$$\frac{k_{-i}}{k_{+i}} \equiv [K_{D,i}] = \frac{[A_{eq}][B_{eq}]}{[A{:}B_{eq}]}. \tag{Def. 1}$$

The dissociation constant for any binding and unbinding reaction i is a measure of how much concentration of the complex $A{:}B$ will dissociate back into A and B. A lower $K_{D,i}$ value indicates stronger binding between the two reactants [7]. Note that the unit of measurement of $K_{D,i}$ is concentration.

Many biological functions, including coagulation, are mediated by enzyme-substrate interactions [19]. In the classical enzyme-substrate reaction, a single

enzyme, denoted as E, binds reversibly to its substrate, referred to as S, resulting in the formation of a complex known as $E{:}S$. This complex $E{:}S$ can dissociate back into either its constituent parts E and S, or E and the newly formed product P if S is successfully converted to P. Subsequently, the unbound E is free for another S to bind it and catalyze a new reaction. This biochemical process is generally described by the following biochemical reaction scheme

$$E + S \underset{k_{-1}}{\overset{k_1}{\rightleftharpoons}} E{:}S \xrightarrow{k_2} E + P. \tag{R3}$$

Here, k_{+1}, k_{-1}, and k_{+2} represent the binding rate, unbinding rate, and catalytic rate, respectively. The catalytic rate k_{+2} measures the efficiency of the enzyme in converting the substrate into the end products, i.e. transforming the S in the complex $E{:}S$ into P. Again, a mathematical model can be obtained using the Law of Mass Action, and the system of ODEs is described as follows:

$$\frac{d[E]}{dt} = -\underbrace{k_{+1}[E][S]}_{\substack{\text{Binding}\\ \text{of } E \text{ to } S}} + \underbrace{k_{-1}[E{:}S].}_{\substack{\text{Unbinding}\\ \text{of } S \text{ from } E{:}S}} + \underbrace{k_{+2}[E{:}S]}_{\substack{\text{Free } E \text{ after}\\ \text{catalyzation}}} \tag{3a}$$

$$\frac{d[S]}{dt} = -\underbrace{k_{+1}[E][S]}_{\substack{\text{Binding}\\ \text{of } E \text{ to } S}} + \underbrace{k_{-1}[E{:}S]}_{\substack{\text{Unbinding}\\ \text{of } S \text{ from } E{:}S}} \tag{3b}$$

$$\frac{d[E{:}S]}{dt} = \underbrace{k_{+1}[E][S]}_{\substack{\text{Binding}\\ \text{of } E \text{ to } S}} - \underbrace{k_{-1}[E{:}S]}_{\substack{\text{Unbinding}\\ \text{of } S \text{ from } E{:}S}} \tag{3c}$$

$$\frac{d[P]}{dt} = \underbrace{k_{+2}[E{:}S].}_{\substack{P \text{ formed after}\\ \text{catalyzation}}} \tag{3d}$$

Note that the unit of measurement for k_{+2} is 1/time.

For the enzyme kinetic reactions described by R3, the Michaelis-Menten constant is defined as a parameter in enzyme kinetics that measures how tightly the substrate binds to the enzyme. It is defined as the substrate concentration at which the reaction rate is half of the maximum reaction rate achieved by the enzyme [14]. The constant K_M has concentration as its units and can be expressed as follows

$$K_M = \frac{k_{-1} + k_{+2}}{k_{+1}}. \tag{Def. 2}$$

For more details about the assumptions and derivation, the reader should refer to [14].

While it is not possible to directly measure the binding rate and unbinding rates in biochemistry and coagulation in general, certain rates/rate combinations can be measured for reacting species, such as the catalytic rate (k_{+2}), the Michaels-Menten constant (K_M), and the dissociation constant ($K_{D,i}$) for a binding and unbinding reaction i. Some reasons why measuring all kinetic

Variables	Definition
S	X
E	TF:VIIa
E:S	TF:VIIa:X
E:P	TF:VIIa:Xa
I	TFPI
P	Xa
P:I	Xa:TFPI
E:P:I	TF:VIIa:Xa:TFPI
P:I:E	TF:VIIa:Xa:TFPI*

Table 1: **Biochemical Species Definition**. Various mechanisms of TFPI inhibition and mathematical models are described/written in terms of the above variables.

rates is biochemically challenging or impossible include system complexities, intermediate reactions/transient species, or experimental constraints.

In my study, for simplicity, I will use the standard Enzyme (E), Substrate (S), Product (P), and inhibitor (I) notation given in Table 1 for the equations and the description that follows. First, the substrate factor X (S) is converted to product Xa (P) by the enzyme TF:VIIa (E). As illustrated in Figure 2, this production is inhibited by the inhibitor TFPI (I) in one of the three complexes: Xa:TFPI (P:I), TF:VIIa:Xa:TFPI (E:P:I), or TF:VIIa:Xa:TFPI*(P:I:E). The latter two are quaternary complexes formed through the interactions of enzyme E with P and I in two different ways: the weaker inhibitory complex, E:P:I consists of direct binding between the complex E:P and I, where I is only binding to P and there is no interaction between E and I (see Figure 2b). On the contrary, the stronger complex, P:I:E has an additional bond between E:I (see Figure 2c). For my study, concentration is measured in nanomolars (nM),

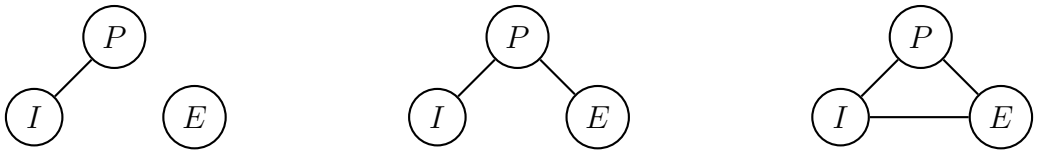

(a) via P:I **(b)** via E:P:I **(c)** via P:I:E

Figure 2: Inhibition of P by I through (a) P:I, (b) E:P:I, and (c) P:I:E

and time is seconds (s).

2.1.2 Background on Experimental Data

Part of the challenge in coagulation and biochemistry more broadly is that it is only possible to measure certain biochemical species [28]. Typically, in experiments, the substrate and enzyme concentrations are combined within a test

tube, and the resulting product's concentration is determined after a specified time interval, sometimes involving preincubation. In a study by Baugh et al.

Variables	IC^{I}(nM)	$IC^{II_{pre}}$(nM)	IC^{II}(nM)
S	170	0	170
E	$\boldsymbol{E}_0$	0	0.128
E:S	0	0	0
E:P	0	0	0
I	2.4	2.4	$\boldsymbol{I}_{post}$
P	0	$\boldsymbol{P}_{pre}$	$\boldsymbol{P}_{post}$
P:I	0	0	$\boldsymbol{P}$**:**$\boldsymbol{I}_{post}$
E:P:I	0	0	0
P:I:E	0	0	0

Table 2: **Initial Conditions for Experimental Data**. IC^{I} represents the initial conditions for *Experiment I:*, in which $\boldsymbol{E}_0$ = [0.1024, 0.512, 0.384, 0.256, 0.192, 0.128, 0.064, 0.032] and all the other variables are fixed. For *Experiment II*, $IC^{II_{pre}}$ represents the initial conditions for the pre-incubation phase in which $\boldsymbol{P}_{pre}$ = [0, 0.25, 0.5, 1] and I is fixed. The set IC^{II} indicates the initial concentrations for post-incubation phase, where $\boldsymbol{I}_{post}$, $\boldsymbol{P}_{post}$, and $\boldsymbol{P}$**:**$\boldsymbol{I}_{post}$ are varied based on post-incubation for fixed S and E.

[2], the formation of Xa (P) was measured over time in the presence of TFPI under two distinct experimental conditions. The first experiment, denoted as *Experiment I*, involved keeping the concentrations of X ($S, 170$nM) and TFPI ($I, 2.4$nM) fixed while varying the concentration of the enzyme TF:VIIa ($\boldsymbol{E}_0$) in the range of 0.032nM to 1.024nM. The second experiment, referred to as *Experiment II*, encompassed two sequential phases. In the initial phase, known as pre-incubation, a fixed TFPI concentration ($I, 2.4$nM) was maintained while the concentrations of Xa ($\boldsymbol{P}_{pre}$) were varied from 0 to 1 nM over a two-hour period. Subsequently, in the post-incubation phase, the resulting mixture derived from the pre-incubation phase, comprising the complex Xa:TFPI ($\boldsymbol{P}$**:**$\boldsymbol{I}_{post}$), TFPI ($\boldsymbol{I}_{post}$), and Xa ($\boldsymbol{P}_{post}$), was combined with a fixed amount of X ($S, 170$nM) and TF:VIIa ($E, 0.128$nM). Finally, the overall concentration of Xa (P) was measured. For both experiments described above, each measurement of Xa is an independent data point. The data itself and the details for the data extraction are given in the Appendix 3.2. The initial conditions for both experiments are given in Table 2.

2.1.3 Background on Previous Modelling Work

While there are different schemes (see Figure 4) that have been used to describe the activation of factor X by TF:VIIa and its inhibition by TFPI, they all have a similar structure. The first biochemical scheme, *Scheme I* (see Figure 4), was proposed by Huang et al. [11] and was investigated by Baugh et al. (1998) [2].

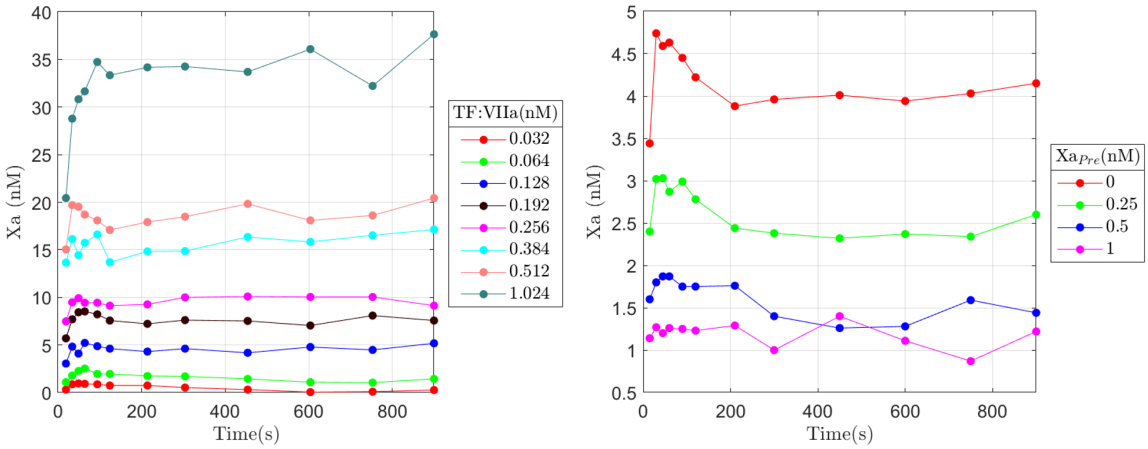

(a) Experiment I **(b)** Experiment II

Figure 3: Experimental Data for Xa formation by Baugh et al. (1998) [2]

In this scheme, the activation of S was described by standard into P, which is instantaneously released from E upon activation. In other words,

$$E + S \rightleftharpoons E{:}S \rightarrow E + P. \tag{4a}$$

The inhibition of P and E by I occurs in two step to form the quaternary complex $P{:}I{:}E$ (see equation 4b-4c). First, I binds to P to generate a complex $P{:}I$ through a reversible biochemical reaction 4b. Then, $P{:}I$ can bind and unbind to E to form the stronger inhibitory complex $P{:}I{:}E$ (4c). This type of TFPI inhibition is called the *Indirect Binding* mechanism

$$P + I \quad \rightleftharpoons \quad P{:}I \tag{4b}$$

$$E + P{:}I \quad \rightleftharpoons \quad P{:}I{:}E. \tag{4c}$$

Baugh et al. [2] could not fit the mathematical model based on *Scheme I* to the experimental data described in section 2.1.2. Instead, they proposed *Scheme II* (see Figure 4), which incorporated two additional sets of assumptions to the existing scheme for product inhibition.
The first assumption considers the inhibition of E by P, that is P can remain bound to E once it is formed and it can unbind and rebind from E (see Equation 5a)

$$E + S \rightleftharpoons E{:}S \rightarrow E{:}P \rightleftharpoons E + P. \tag{5a}$$

The second assumption proposes that I may also bind to P while P is still bound to E (i.e. to the complex $E{:}P$) creating the complex $E{:}P{:}I$ (see Equation 5b). The latter quaternary complex can be described as a weaker form of inhibition:

$$E{:}P + I \rightleftharpoons E{:}P{:}I. \tag{5b}$$

Furthermore, the complex $E{:}P{:}I$ would then allow the stronger complex, $P{:}I{:}E$ to form in two different ways. One way $P{:}I{:}E$ can be formed is by the unbinding

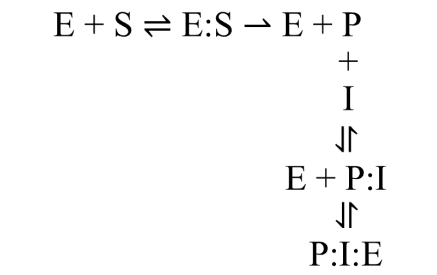

Scheme I

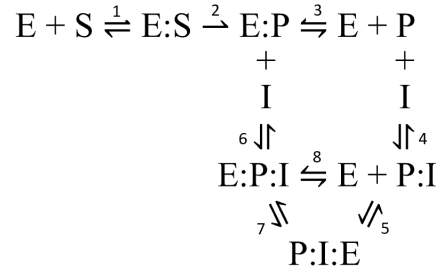

Scheme II

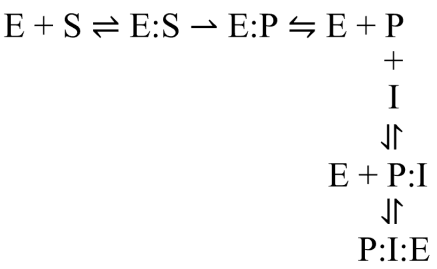

Scheme III

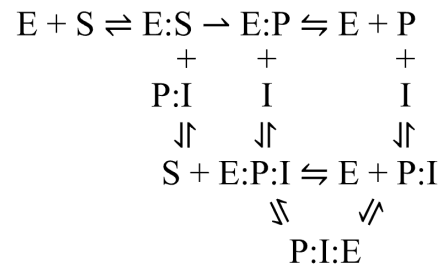

Scheme IV

Figure 4: Biochemical Schemes for Xa formation and TFPI Inhibition: *Scheme I* was suggested by Huang et al. (1993) [11] and was studied by Baugh et. al.(1998) [2]. *Scheme II* was proposed by Baugh et. al. (1998) [2]but never studied. *Scheme III* and *Scheme IV* were examined by Panteleev et al. (2002) [26].

of P:I from E in the complex E:P:I. Then, the complex P:I can rebind to E to form the stronger complex P:I:E.

$$E{:}P{:}I \rightleftharpoons E + P{:}I \rightleftharpoons P{:}I{:}E. \tag{5c}$$

Another way P:I:E can be formed is by an isomerization where there is a transition between the two complexes as follows

$$E{:}P{:}I \rightleftharpoons P{:}I{:}E. \tag{5d}$$

Even though the *Scheme II* was not studied by Baugh et al., it was further explored in another study by Panteleev et al. [26]. The latter analyzed several mathematical models which included *Scheme II* and proposed two additional schemes *Scheme III* and *Scheme IV* presented in Figure 4 to describe the inhibition of E by I [26]. The *Scheme III*, which was a modified version of *Scheme II*, considered the inhibition of P by E as represented in Equation 5a but did not include direct inhibition of E by I represented by Equations 5b-5d. And, *Scheme IV* was a replicate of *Scheme II* with an additional assumption which included the displacement of S with P:I while S is still bound to E to form the complex E:P:I as represented by Equation 6a.

$$E{:}S + P{:}I \rightleftharpoons S + E{:}P{:}I. \tag{6a}$$

In their study, Panteleev et al. examined different schemes to determine which scheme could fit the data measured in *Experiment I* and *Experiment II* simultaneously and was capable of describing the experiments quantitatively. They concluded *Scheme II* is not the right scheme to explain experimental data because it not only fit the data poorly but also could not even order the experimental curves same way as measured. They also reported that the *Scheme III* was too weak to inhibit the factor P activation by I and could not describe the experimental data [26]. They suggested that the only way the data could fit and be ordered consistently was by invoking a trimolecular reaction (see Equation 6a). However, the data from molecular models (crystal structure) suggest that these trimolecular reactions would be rare [23]. Moreover, the fitted kinetic rates for the *Scheme IV* were inconsistent with the experimentally measured rates and constants.

For my study, I hypothesized that *Scheme II* could describe the role of TFPI in regulating the activation of factor X. I developed a mathematical model based on *Scheme II*, which incorporated both *Direct Binding* and *Indirect Binding* mechanisms for TFPI inhibition. I hypothesized that the reason why previous studies were unsuccessful at fitting experimental data (described in Section 2.1.2) using a mathematical model based on *Scheme II* is the choice of kinetic rates. Instead, I estimated a set of kinetic rates that fitted the model output for P to the experimental data simultaneously. This involved employing a constraints optimization framework, leveraging existing knowledge about certain kinetic rates, and re-estimating the dissociation constant for reaction (4b).

2.2 TFPI ODEs Static Model

2.2.1 Mathematical Model

The TFPI ODEs Static model based on *Scheme II* in Figure 4 tracks the species concentrations for nine species ($[E]$, $[S]$, $[E{:}S]$, $[E{:}P]$, $[P]$, $[I]$, $[P{:}I]$, $[P{:}I{:}E]$, and $[E{:}P{:}I]$) over time. By applying the Law of Mass Action, one can derive the system of ODEs for the concentrations of species for *Scheme II* as follows:

$$\frac{d[E]}{dt} = \underbrace{-k_{+1}[E][S]}_{\substack{\text{Binding}\\ \text{of } S \text{ to } E}} \underbrace{+k_{-1}[E{:}S]}_{\substack{\text{Unbinding}\\ \text{of } S \text{ from } E}} \underbrace{+k_{-3}[E{:}P]}_{\substack{\text{Unbinding}\\ \text{of } P \text{ from } E{:}P}} \underbrace{-k_{+3}[E][P]}_{\substack{\text{Binding}\\ \text{of } P \text{ to } E}} \underbrace{-k_{+5}[E][P{:}I]}_{\substack{\text{Binding}\\ \text{of } P{:}I \text{ to } E}} \underbrace{+k_{-5}[P{:}I{:}E]}_{\substack{\text{Unbinding}\\ \text{of } P{:}I \text{ from } E}} \underbrace{+k_{-8}[E{:}P{:}I]}_{\substack{\text{Unbinding}\\ \text{of } P{:}I \text{ from } E{:}P{:}I}} \underbrace{-k_{+8}[E][P{:}I]}_{\substack{\text{Binding}\\ \text{of } P{:}I \text{ to } E}} \tag{7a}$$

$$\frac{d[S]}{dt} = \underbrace{-k_{+1}[E][S]}_{\substack{\text{Binding}\\ \text{of } S \text{ to } E}} \underbrace{+k_{-1}[E{:}S]}_{\substack{\text{Unbinding}\\ \text{of } S \text{ from } E}} \tag{7b}$$

$$\frac{d[E{:}S]}{dt} = \underbrace{k_{+1}[E][S]}_{\substack{\text{Binding}\\ \text{of } S \text{ to } E}} \underbrace{-k_{-1}[E{:}S]}_{\substack{\text{Unbinding}\\ \text{of } S \text{ from } E}} \underbrace{-k_{+2}[E{:}S]}_{\substack{\text{catalyzation}\\ \text{of } S \text{ to } P}} \tag{7c}$$

$$\frac{d[E{:}P]}{dt} = \underbrace{k_{+2}[E{:}S]}_{\substack{\text{catalyzation}\\ \text{of } S \text{ to } P}} \underbrace{-k_{-3}[E{:}P]}_{\substack{\text{Unbinding}\\ \text{of } P \text{ from } E}} \underbrace{+k_{+3}[E][P]}_{\substack{\text{Binding}\\ \text{of } P \text{ to } E}} - \underbrace{k_{+6}[E{:}P][I]}_{\substack{\text{Binding}\\ \text{of } I \text{ to } E{:}P}} + \underbrace{k_{-6}[E{:}P{:}I]}_{\substack{\text{Unbinding}\\ \text{of } I \text{ from } E{:}P}} \tag{7d}$$

$$\frac{d[P]}{dt} = \underbrace{-k_{+3}[E][P]}_{\substack{\text{Binding}\\ \text{of } P \text{ to } E}} \underbrace{+k_{-3}[E{:}P]}_{\substack{\text{Unbinding}\\ \text{of } P \text{ from } E}} \underbrace{-k_{+4}[P][I]}_{\substack{\text{Binding}\\ \text{of } I \text{ to } P}} + \underbrace{k_{-4}[P{:}I]}_{\substack{\text{Unbinding}\\ \text{of } I \text{ from } P}} \tag{7e}$$

$$\frac{d[I]}{dt} = \underbrace{-k_{+4}[P][I]}_{\substack{\text{Binding}\\ \text{of } I \text{ to} P}} + \underbrace{k_{-4}[P{:}I]}_{\substack{\text{Unbinding}\\ \text{of } I \text{ from } P}} \underbrace{-k_{+6}[E{:}P][I]}_{\substack{\text{Binding}\\ \text{of } I \text{ to } E{:}P}} \underbrace{+k_{-6}[E{:}P{:}I]}_{\substack{\text{Unbinding}\\ \text{of } I \text{ from } E{:}P}} \tag{7f}$$

$$\frac{d[P{:}I]}{dt} = \underbrace{k_{+4}[P][I]}_{\substack{\text{Binding}\\ \text{of } I \text{ to } P}} \underbrace{-k_{-4}[P{:}I]}_{\substack{\text{Unbinding}\\ \text{of } I \text{ from } P}} \underbrace{-k_{+5}[E][P{:}I]}_{\substack{\text{Binding}\\ \text{of } P{:}I \text{ to } E}} \underbrace{+k_{-5}[P{:}I{:}E]}_{\substack{\text{Unbinding}\\ \text{of } P{:}I \text{ to } E}} \underbrace{-k_{+8}[E][P{:}I]}_{\substack{\text{Binding}\\ \text{of } P{:}I \text{ to } E}} + \underbrace{k_{-8}[E{:}P{:}I]}_{\substack{\text{Unbinding}\\ \text{of } P{:}I \text{ from } E}} \tag{7g}$$

$$\frac{d[E{:}P{:}I]}{dt} = \underbrace{k_{+6}[E{:}P][I]}_{\substack{\text{Binding}\\ \text{of } P{:}I \text{ to } E}} \underbrace{-k_{-6}[E{:}P{:}I]}_{\substack{\text{Unbinding}\\ \text{of } P{:}I \text{ from } E}} \underbrace{-k_{+7}[E{:}P{:}I]}_{\substack{\text{Transition of}\\ E{:}P{:}I \text{ to } P{:}I{:}E}} \underbrace{+k_{-7}[P{:}\,I{:}E]}_{\substack{\text{Transition of}\\ P{:}I{:}E \text{ to } E{:}P{:}I}} \underbrace{+k_{+8}[E][P{:}I]}_{\substack{\text{Binding}\\ \text{of } P{:}I \text{ to } E}} - \underbrace{k_{-8}[E{:}P{:}I]}_{\substack{\text{Unbinding}\\ \text{of } P{:}I \text{ to } E}} \tag{7h}$$

$$\frac{d[P{:}I{:}E]}{dt} = \underbrace{k_{+5}[E][P{:}I]}_{\substack{\text{Binding}\\ \text{of} P{:}I \text{ to } E}} \underbrace{-k_{-5}[P{:}I{:}E]}_{\substack{\text{Unbinding}\\ \text{of } P{:}I \text{ from } E}} \underbrace{+k_{+7}[E{:}P{:}I]}_{\substack{\text{Transition of}\\ P{:}I{:}E \text{ to } E{:}P{:}I}} \underbrace{-k_{-7}[P{:}I{:}E]}_{\substack{\text{Transition of}\\ P{:}I{:}E \text{ to } E{:}P{:}I}}. \tag{7i}$$

Here, the $k_{\pm i}$ excluding k_{-2} represent the kinetic rates for the reactionumber $i = 1, 2, 3, 4, 5, 6, 7, 8$. In particular, the rates for reactions $i = 1, 3, 4, 5, 6, 8$ are binding $(+)$ and unbinding $(-)$, k_{+2} is the catalytic rate, and $k_{\pm 7}$ are the transitioning rates between complexes $E{:}P{:}I$ and $P{:}I{:}E$.

I assume that $E{:}P{:}I$ is an internally weaker complex because it has only two points of interactions as illustrated in Figure 2b and $P{:}I{:}E$ is an internally stronger complex because it has three points of interactions as depicted in Figure 2c. Furthermore, I assume the formation of $P{:}I{:}E$ through $E{:}P{:}I$ complex is rapid. I hypothesize that the transition from the stronger complex $P{:}I{:}E$ to

the weaker complex $E{:}P{:}I$ is significantly slower as described by Baugh et. al [2]. In other words,

$$k_{-7} \ll k_{+7}. \tag{8}$$

2.2.2 Parameter Estimation

Prior Information about the Kinetic Rates

The TFPI ODEs Static model has fifteen distinct kinetic rates $k_{\pm i}$ (excluding k_{-2}), where $i = 1, 2, ..., 8$, describing the eight biochemical reactions illustrated in *Scheme II*. For my research, I relied on previously reported values of k_{+5}, k_{-5}, and K_M measured by Baugh et al. [2]. In their study, Baugh et al. also determined the value of $K_{D,4}$ and provided the data used for its measurement. I utilized this data to re-evaluate the value of $K_{D,4}$ (see Appendix 3.1 for details) and observed that my estimated value diverged from their reported value. Consequently, I adopted my newly estimated value for my study.

Furthermore, I used the experimentally measured dissociation constant $K_{D,3}$ from the study conducted by Lu et al. [17]. I leveraged the knowledge of both $K_{D,3}$ and $K_{D,4}$ by applying the definition of the dissociation constant (Def. 1) to calculate the corresponding unbinding rates, k_{-3} and k_{-4}, in relation to the given binding rates, k_{+3} and k_{+4}, respectively. Similarly, I used the known K_M and its definition (Def. 2) to determine k_{-1} for a given k_{+1} and k_{+2}.

In summary, I considered rates k_{-1}, k_{-3}, k_{-4}, k_{+5}, and k_{-5} to be known based on their reported values or their relationship to known constants from literature. I estimated the remaining ten unknown kinetic rates $\boldsymbol{\theta} = k_{+1}$, k_{+2}, k_{+3}, k_{+4}, k_{+6}, k_{-6}, k_{+7}, k_{-7}, k_{+8}, and k_{-8} using a constrained optimization method described below. For detailed information on all the kinetic rates, please refer to Table 3.

Constrained Optimization Method

The goal was to estimate a set of kinetic rates $\boldsymbol{\theta}$ that fits the ODEs Static model to the experimental data described in section 2.1.2. This involved minimizing the error between the experimental data and the model's approximation of Xa (P) concentration, while simultaneously ensuring that all constraints based on biological concepts and prior knowledge were met. Essentially to find such $\boldsymbol{\theta}$, I had to solve the following minimization problem

$$\min_{\boldsymbol{\theta}} f(\boldsymbol{\theta}) \; \textit{such that} \begin{cases} C_I(x) \leq 0 \\ C_E(x) = 0. \end{cases} \tag{9}$$

Here, $f(\boldsymbol{\theta})$ represents the objective function responsible for quantifying the error between the data and the model's output ($[P]$), which depends on the values of $\boldsymbol{\theta}$. Meanwhile, the constraints $C_E(x)$ and $C_I(x)$ are the inequality and equality constraints, respectively. Both the objective function and constraints are described further below.

To tackle this minimization problem, I employed a constrained optimization framework. The latter, in general, is a branch of mathematical optimization

focused on maximizing or minimizing an objective function with respect to some variables while respecting constraints within the feasible region defined by those constraints themselves [22]. The commonly used techniques for solving constrained optimization problems include the interior point method or sequential programming. For this project, I utilized the interior point method, a class of algorithms designed for solving linear and non-linear optimization problems of minimization or maximization [22]. This method transforms the contained problem into an unconstrained optimization problem by introducing barrier functions, and it uses Newton's methods to solve it. For the detailed algorithm, please refer to Appendix 3.3. Some advantages of using the interior point method include: robustness, feasibility guarantee, and being well-suited for solving large-scale linear/nonlinear programming problems.

For the ODEs Static model, the constraints are described as follows.

Constraint 1. All the kinetic rates must be positive. This means

$$k_i \geq 0, \tag{10}$$

for all $i = \pm 1, 2, \pm 3, \cdots, \pm 8$.

Constraint 2. Because there is a limit on how fast particles can diffuse, Alberty et al. estimated an upper limit of enzyme-substrate reaction using the theory of diffusion-controlled reaction [1]. According to their estimation, the upper limit of enzyme-substrate reaction was $10^9 \mathrm{M}^{-1} \times s^{-1}$. Thus, I assumed that all the binding rates k_{+i} are bounded above by $1\mathrm{nM}^{-1} \times s^{-1}$, so

$$0 \leq k_i \leq 1, \tag{11}$$

where for $i = 1, 3, 4, 5, 6, 8$.

Constraint 3. Recall the assumption that the transitioning rate k_{-7} is significantly smaller than k_{+7} as described by inequality (8). One way to enforce this constraint is by choosing feasible ranges for k_{+7} and k_{-7} such that the inequality (8) is true. I assume that

$$0 \leq k_{+7} \leq 10^3 \text{ and } 10^{-9} \leq k_{-7} \leq 10^{-4}. \tag{12}$$

These ranges were chosen for k_{+7} and k_{-7} based on my numerical experiments of the model.

Constraint 4. The linear inequality constraint described below was formulated by combining the definition of the Michaelis-Menten constant (see Def. 2) and the positivity of k_{-1} from inequality (10).

$$-K_M k_1 + k_2 \leq 0. \tag{13}$$

The derivation of the above inequality is as follows:

$$\begin{aligned}
K_M = \frac{k_{-1} + k_2}{k_1} \quad & \text{Definition of } K_M \\
K_M k_1 - k_2 = k_{-1} \quad & \text{Solved for } k_{-1} \\
K_M k_1 - k_2 = k_{-1} \geq 0 \quad & \text{from inequality (10)} \\
-K_M k_1 + k_2 = k_{-1} \leq 0 \quad & \text{Multiplied by -1.}
\end{aligned}$$

The objective function used for the estimation of the kinetic rates is given by the Sum of Squares Error, $f(\boldsymbol{\theta})$, which measures the difference between experimental data and predicted model output [4]. The function $f(\boldsymbol{\theta})$ for fitting time series data from *Experiment I* and *Experiment II* simultaneously is defined as follows:

$$f(\boldsymbol{\theta}) = \left(\underbrace{\frac{1}{96}\sum_{k=1}^{8}\sum_{i=1}^{12}\left(D_{i,k}^{I} - P_{i,k}^{I}(t_i^I, IC_k^I, \boldsymbol{\theta})\right)^2}_{Experiment\ I} + \underbrace{\frac{1}{48}\sum_{n=1}^{4}\sum_{m=1}^{12}\left(D_{m,n}^{II} - P_{m,n}^{II}(t_m^{II}, IC_n^{II}, \boldsymbol{\theta})\right)^2}_{Experiment\ II} \right)^{1/2}. \tag{14}$$

Here, $D_{i,k}^{I}$ and $P_{i,k}^{I}(t_i^I, IC_k^I, \boldsymbol{\theta})$ represent the experimental data point and the corresponding ODE model solution respectively at discrete time point t_i^I and the initial species' concentrations IC_k^I for *Experiment I*. Similarly, $D_{m,n}^{2}$ and $P_{m,n}^{II}(t_m^{II}, IC_n^{II}, \boldsymbol{\theta})$ indicate the experimental data and the corresponding ODE model solution at the discrete time point t_m^{II} and the initial species' concentrations IC_n^{II} *Experiment II*.

My goal is to find a set of the kinetic rates $\boldsymbol{\theta}$ that minimizes the objective function $\boldsymbol{f(\theta)}$, subject to the constraints. Mathematically, I want to solve the following minimization problem

$$\min_{\boldsymbol{\theta}} f(\boldsymbol{\theta})\ such\ that \begin{cases} k_i >= 0,\ \forall i = i = \pm 1, 2, \pm 3, \cdots, \pm 8. \\ 0 \le k_i \le 1,\ \forall i = 1, 3, \cdots, 6, 8. \\ 0 \le k_7 \le 10^3. \\ 10^{-9} \le k_{-7} \le 10^{-4}. \\ -K_M k_1 + k_2 \le 0. \end{cases} \tag{15}$$

To solve this problem, I adopted MATLAB built-in nonlinear constrained optimization [12] function `fmincon`, which uses the interior point method by default. This function starts at a vector of initial guesses $\boldsymbol{\theta}_0$ sampled randomly from a uniform distribution. The feasible ranges for parameters in the vector $\boldsymbol{\theta}$ are defined by lower bounds and upper bounds, taking into account the constraints (10), (11), and (12) associated with the kinetic rates. The function searches for the optimal set of kinetic rates $\boldsymbol{\theta}_{min}$ that minimizes the error calculated by the objective function (described in equation 14) subject to the linear inequalities $-K_M k_1 + k_2 \le 0$. For my study, I did 1000 realization to find $\boldsymbol{\theta}_{min}$. The details about the feasible ranges, parameters relationships, and optimized kinetic rates are provided in Table 3.

Though `fmincon.m` is a useful MATLAB optimization tool designed for constrained nonlinear problems, it also has notable limitations, some of which are described as follows. First, it relies on the user-provided initial guesses, which can significantly affect the optimization output by making the latter sensitive to the choice of initial guess. Second, it requires the objective function and constraints must have continuous and continuous first derivatives. Third, it might not handle problems with numerous variables or constraints efficiently.

Moreover, it attempts to minimize the maximum constraint value when the problem is infeasible. Lastly, it may not guarantee a global optimality for complex optimization problems, so the user should seek other global optimization techniques. [12]

2.2.3 Results

Numerical simulations for the concentration of P were performed by fitting the TFPI ODEs Static model to experimental data (described in Section 2.1.2) simultaneously using a constrained optimization framework (see Section 2.2.2). Figure 5 illustrates the comparison between the model solution for the concentration of P and the corresponding experimental data. In *Experiment I* (Figure 5a), I kept the concentrations of S and I constant at 170 nM and 2.4 nM, respectively, and varied the initial concentration of E. In *Experiment II* (5b), I fixed E at 0.128 nM and S at 170 nM. The complex P:I and I were obtained by preincubating fixed I at 2 nM with various P concentrations of 0, 0.25, 0.5, and 1 nM.

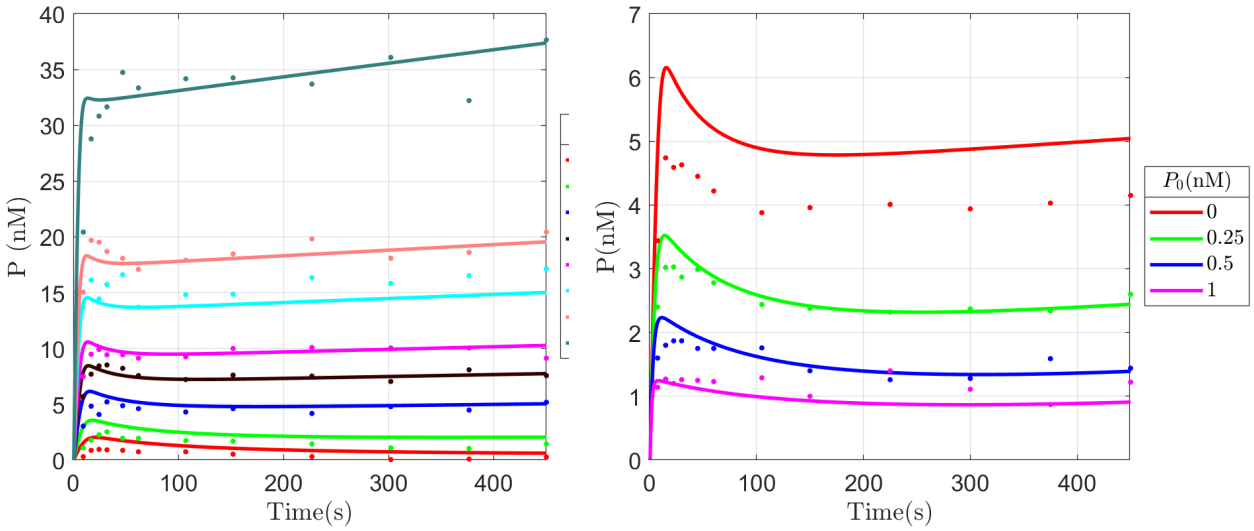

(a) *Experiment II* **(b)** *Experiment II*

Figure 5: Numerical simulations (solid lines) and extracted experimental data (solid dots) of P concentrations given fixed concentrations of factor $S = 170$ nM using optimized kinetic rates (See Table 2). (a) The concentration of I is fixed at 2.4 nM, whereas the concentration of E is varied. (b) E is fixed to 0.128 nM. I, P, and P:I concentrations are varied based on the preincubation from fixed I under various P initial concentrations.

In Figure 5, it can be observed that the TFPI ODEs Static model fits most of the data from *Experiment I* and *Experiment II* simultaneously. In particular, the bottom two curves associated with ($E_0 = 0.032$nM and $E_0 = 0.064$nM) for *Experiment I* and the top curve for *Experiment II* are overestimated. The set of

Table 3: **Scheme Reactions and the Associated Kinetic Rates**

Reaction Number	Biochemical Equation	Kinetic Constants	Units	Literature Value	Optimized Value	Feasible Ranges
1	$E + S \underset{k_{-1}}{\overset{k_1}{\rightleftharpoons}} E{:}S$	k_{+1}	$(nMs)^{-1}$	-	1.9×10^{-1}	$[k_{+2}/K_M, 1]^a$
		k_{-1}	s^{-1}	-	3.6×10^{1}	$K_M \times k_{+1} - k_{+2}$
		K_M	nM	2.38×10^2 [2]	-	-
		$K_{D,1}$	nM	-	191	-
2	$E{:}S \xrightarrow{k_2} E{:}P$	k_{+2}	s^{-1}	–	9	$[0, 10]^b$
3	$E + P \underset{k_{-3}}{\overset{k_3}{\rightleftharpoons}} E{:}P$	k_{+3}	$(nMs)^{-1}$	-	2.4×10^{-1}	$[0, 1]^a$
		k_{-3}	s^{-1}	-	1.24×10^2	$K_{D,3} \times k_{+3}$
		$K_{D,3}$	nM	5.21×10^2 [17]	-	-
4	$P + I \underset{k_{-4}}{\overset{k_4}{\rightleftharpoons}} P{:}I$	k_{+4}	$(nMs)^{-1}$	-	2.1×10^{-3}	$[0, 1]^a$
		k_{-4}	s^{-1}	-	5.4×10^{-5}	$K_{D,4} \times k_{+4}$
		$K^c_{D,4}$	nM	-	2.6×10^{-2}	-
5	$E + P{:}I \underset{k_{-5}}{\overset{k_5}{\rightleftharpoons}} P{:}I{:}E$	k_{+5}	$(nMs)^{-1}$	7.34×10^{-3} [2]	-	-
		k_{-5}	s^{-1}	1.1×10^{-3} [2]	-	-
		$K^*_{D,5}$	nM	1.5×10^{-1} [2]	-	-
6	$E{:}P + I \underset{k_{-6}}{\overset{k_6}{\rightleftharpoons}} E{:}P{:}I$	k_{+6}	$(nMs)^{-1}$	-	3.6×10^{-1}	$[0, 1]^a$
		k_{-6}	s^{-1}	-	1	$[0, 10]^b$
		$K_{D,6}$	nM	-	2.8	-
7	$E{:}P{:}I \underset{k_{-7}}{\overset{k_7}{\rightleftharpoons}} P{:}I{:}E$	k_{+7}	s^{-1}	-	2.1×10^2	$[0, 10^3]^b$
		k_{-7}	s^{-1}	-	1.6×10^{-4}	$[1 \times 10^{-7}, 1 \times 10$
		$K_{D,7}$	-	-	-	-
8	$E + P{:}I \underset{k_{-8}}{\overset{k_8}{\rightleftharpoons}} E{:}P{:}I$	k_{+8}	$(nMs)^{-1}$	-	6.7×10^{-1}	$[0, 1]^a$
		k_{-8}	s^{-1}	-	1.2	$[0, 100]^b$
		$K_{D,8}$	nM	-	1.8	-

[a] The upper bound was selected to be equal to 1 nM due to the diffusion limit of the rate of association. The lower bound was chosen to be equal to zero since we are dealing with biological parameters (except k_{+1} has a lower limit of K_M/k_{+2} because it depends on the Michaelis–Menten constant and catalytic rate k_{+2}).
[b] Assumed.
[c] Optimized (see Appendix).
* calculated using the formula k_{-5}/k_{+5}.

kinetic rates used for the fitting was obtained through constrained optimization and is described in 3). The optimized set of parameters was consistent with all the prior knowledge.

Overall, it can be observed that the model output for the concentration of P explains the qualitative behavior of each experimental data set because the ordering and the shape of the curves are consistent with the experimental data. This stands out as a novel development, as the earlier study conducted by Panteleev et al. was not able to achieve this level of consistency. Moreover, my results show the importance of having the *Direct Binding* mechanism in *Scheme II* static conditions because the model fitted the experimental data using both mechanisms.

2.3 TFPI ODEs Flow Model

While the previous sections have uncovered kinetic parameters for a static model incorporating both TFPI *Direct Binding* and *Indirect Binding* inhibition mechanisms, a complete study should consider how the system behaves under flow because the coagulation process occurs in the presence of flow [16]. This section aims to develop an ODEs flow model to understand how *Direct Binding* and *Indirect Binding* mechanisms interact in an actual physical system. I hypothesize that the *Direct Binding* mechanism is essential for TF:VIIa inhibition in the presence of flow because it allows the inhibitor TFPI to bind with Xa, while the latter is bound to TF:VIIa.

2.3.1 Biological and Modelling of the ODEs Flow Model

My model for Xa activation and TFPI inhibition in the presence of flow, as illustrated by Figure 6, is a simplified version of the previously developed mathematical model of flow-mediated coagulation by Fogelson group [15, 10] with minimal reacting species of interest. The model assumes that all the reactions happen in a region located at the small ($10\mu M \times 10\mu M$) [10] injury site, this region is called the reaction zone. Clotting factors are transported into and out of the reaction zone by a combination of flow and diffusion, represented by a mass transfer coefficient (called "flow rate" and denoted k_{flow}). The value of k_{flow} (1/s) is given by the function that depends on vessel size, injury length, blood flow speed, and the species' diffusivity [15, 10]. Since I am working with a small injury, it is assumed that all the species are well mixed in the reaction zone, so each is characterized by its (volume) concentration. Inside the reaction zone, the clotting factors' concentrations change due to their interactions with other species through biochemical reactions (in fluid or on the surface) and their transport into and out of the reaction zone.

My model assumes that the TF:VIIa (E) is already formed and is fixed to the injury site inside the reaction zone and does not enter or exit it. The clotting factors that enter the reaction zone are factor X (S_{up}) and the inhibitor TFPI (I_{up}). The ones that exit the reaction zone are X (S), Xa (P), TFPI (I), and Xa:TFPI (P:I). The system becomes inhibited when TF:VIIa is bound

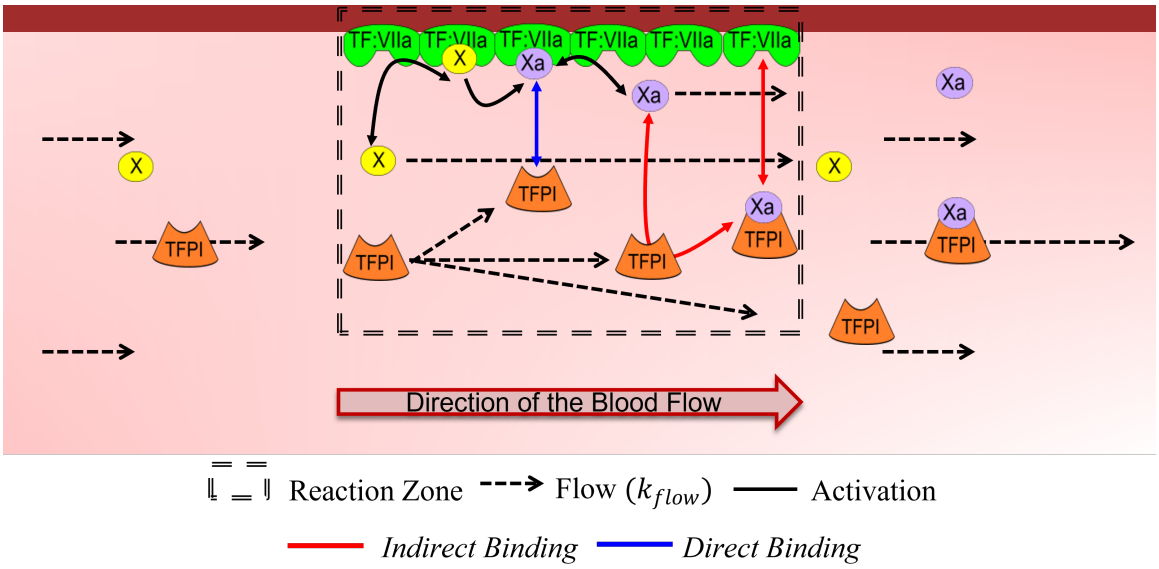

Figure 6: Activation of Xa and Inhibition by TFPI under Flow. During the initiation process, clotting factor X, present in the plasma, becomes activated factor X (Xa) by binding with TF:VIIa. TFPI inhibits this activation through two different biochemical mechanisms: *Indirect Binding* (in red) and *Direct Binding* (in blue). The blood flow (k_{flow}) serves as a mediator for bringing in and removing biochemical components present in the plasma from the reaction zone. The formation of Xa and its inhibition occurs at respective kinetic rates given in Table 3.

by other species, which prevents it from binding and activating factor X. This includes TF:VIIa binding with Xa or Xa:TFPI. Furthermore, recall that there are two mechanisms (*Indirect Binding* and *Direct Binding*) by which TFPI acts to inhibit the action of TF:VIIa after activation of factor X as depicted in Figure 6. The *Indirect Binding* mechanism occurs in two steps: the first step happens in the solution, where TFPI binds to Xa; and in the second step, occurring on the surface of the injury site, the TFPI:Xa complex rebinds to the TF:VIIa complex at the injury site. The *Indirect Binding* mechanism is sensitive to flow because it requires the binding of TFPI and Xa in plasma (hypothesis). On the contrary, the *Direct Binding* mechanism occurs through the direct binding at the injury site of TFPI to the Xa on the TF:VIIa complex immediately after the activation of factor X (i.e., factor Xa never detaches from TF:VIIa to the injury site). Per se, it removes the potential inhibition of Xa:TFPI by the flow.

2.3.2 Mathematical Model

For the description of my mathematical model and the results that follow, I will use the same notation for biochemical species as described in Table 1. The new model, named TFPI ODEs Flow Model, is an open system and is represented mathematically as a compartment model system where species enter and exit the compartment (the reaction zone). The mathematical equations for all the reactions happening inside the reaction zone are the same as the differential equations described previously by (7a-7i) for the ODEs static model (i.e. closed system see Section 2.2.1). The species entering or exiting the reaction zone at rate $k_{flow}(1/s)$ are described by $k_{flow}(C_{up}-C)$, where k_{flow} is the mass transfer coefficient, C_{up} is the upstream concentration of an arbitrary species C, and C is unbound species in the fluid. The full set of ordinary differential equations

for the TFPI ODEs Flow Model is as follows:

$$\frac{d[E]}{dt} = \underbrace{-k_{+1}[E][S]}_{\substack{\text{Binding}\\ \text{of } S \text{ to } E}} \underbrace{+k_{-1}[E{:}S]}_{\substack{\text{Unbinding}\\ \text{of } S \text{ from } E}} \underbrace{+k_{-3}[E{:}P]}_{\substack{\text{Unbinding}\\ \text{of } P \text{ from } E{:}P}} \underbrace{-k_{+3}[E][P]}_{\substack{\text{Binding}\\ \text{of } P \text{ to } E}} \underbrace{-k_{+5}[E][P{:}I]}_{\substack{\text{Binding}\\ \text{of } P{:}I \text{ to } E}} \underbrace{+k_{-5}[P{:}I{:}E]}_{\substack{\text{Unbinding}\\ \text{of } P{:}I \text{ from } E}} \underbrace{+k_{-8}[E{:}P{:}I]}_{\substack{\text{Unbinding}\\ \text{of } P{:}I \text{ from } E{:}P{:}I}} \underbrace{-k_{+8}[E][P{:}I]}_{\substack{\text{Binding}\\ \text{of } P{:}I \text{ to } E}} \tag{16a}$$

$$\frac{d[S]}{dt} = \underbrace{-k_{+1}[E][S]}_{\substack{\text{Binding}\\ \text{of } S \text{ to } E}} \underbrace{+k_{-1}[E{:}S]}_{\substack{\text{Unbinding}\\ \text{of } S \text{ from } E}} + \underbrace{k_{flow}([S_{up}] - [S])}_{\substack{\text{Difference in } [S]\\ \text{due to } k_{flow}}} \tag{16b}$$

$$\frac{d[E{:}S]}{dt} = \underbrace{k_{+1}[E][S]}_{\substack{\text{Binding}\\ \text{of } S \text{ to } E}} \underbrace{-k_{-1}[E{:}S]}_{\substack{\text{Unbinding}\\ \text{of } S \text{ from } E}} \underbrace{-k_{+2}[E{:}S]}_{\substack{\text{catalyzation}\\ \text{of } S \text{ to } P}} \tag{16c}$$

$$\frac{d[E{:}P]}{dt} = \underbrace{k_{+2}[E{:}S]}_{\substack{\text{catalyzation}\\ \text{of } S \text{ to } P}} \underbrace{-k_{-3}[E{:}P]}_{\substack{\text{Unbinding}\\ \text{of } P \text{ from } E}} \underbrace{+k_{+3}[E][P]}_{\substack{\text{Binding}\\ \text{of } P \text{ to } E}} - \underbrace{k_{+6}[E{:}P][I]}_{\substack{\text{Binding}\\ \text{of } I \text{ to } E{:}P}} + \underbrace{k_{-6}[E{:}P{:}I]}_{\substack{\text{Unbinding}\\ \text{of } I \text{ from } E{:}P}} \tag{16d}$$

$$\frac{d[P]}{dt} = \underbrace{-k_{+3}[E][P]}_{\substack{\text{Binding}\\ \text{of } P \text{ to } E}} \underbrace{+k_{-3}[E{:}P]}_{\substack{\text{Unbinding}\\ \text{of } P \text{ from } E}} \underbrace{-k_{+4}[P][I]}_{\substack{\text{Binding}\\ \text{of } I \text{ to } P}} + \underbrace{k_{-4}[P{:}I]}_{\substack{\text{Unbinding}\\ \text{of } I \text{ from } P}} - \underbrace{k_{flow}[P]}_{\substack{\text{Removal of } P\\ \text{due to flow}}} \tag{16e}$$

$$\frac{d[I]}{dt} = \underbrace{-k_{+4}[P][I]}_{\substack{\text{Binding}\\ \text{of } I \text{ to} P}} + \underbrace{k_{-4}[P{:}I]}_{\substack{\text{Unbinding}\\ \text{of } I \text{ from } P}} \underbrace{-k_{+6}[E{:}P][I]}_{\substack{\text{Binding}\\ \text{of } I \text{ to } E{:}P}} \underbrace{+k_{-6}[E{:}P{:}I]}_{\substack{\text{Unbinding}\\ \text{of } I \text{ from } E{:}P}} + \underbrace{k_{flow}([I_{up}] - [I])}_{\substack{\text{Difference in } [I]\\ \text{due to } k_{flow}}} \tag{16f}$$

$$\frac{d[P{:}I]}{dt} = \underbrace{k_{+4}[P][I]}_{\substack{\text{Binding}\\ \text{of } I \text{ to } P}} \underbrace{-k_{-4}[P{:}I]}_{\substack{\text{Unbinding}\\ \text{of } I \text{ from } P}} \underbrace{-k_{+5}[E][P{:}I]}_{\substack{\text{Binding}\\ \text{of } P{:}I \text{ to } E}} \underbrace{+k_{-5}[P{:}I{:}E]}_{\substack{\text{Unbinding}\\ \text{of } P{:}I \text{ to } E}} \underbrace{-k_{+8}[E][P{:}I]}_{\substack{\text{Binding}\\ \text{of } P{:}I \text{ to } E}} + \underbrace{k_{-8}[E{:}P{:}I]}_{\substack{\text{Unbinding}\\ \text{of } P{:}I \text{ from } E}} - \underbrace{k_{flow}[P{:}I]}_{\substack{\text{Removal of } P{:}I\\ \text{due to } k_{flow}}} \tag{16g}$$

$$\frac{d[E{:}P{:}I]}{dt} = \underbrace{k_{+6}[E{:}P][I]}_{\substack{\text{Binding}\\ \text{of } P{:}I \text{ to } E}} \underbrace{-k_{-6}[E{:}P{:}I]}_{\substack{\text{Unbinding}\\ \text{of } P{:}I \text{ from } E}} \underbrace{-k_{+7}[E{:}P{:}I]}_{\substack{\text{Transition of}\\ E{:}P{:}I \text{ to } P{:}I{:}E}} \underbrace{+k_{-7}[P{:}\,I{:}E]}_{\substack{\text{Transition of}\\ P{:}I{:}E \text{ to } E{:}P{:}I}} \underbrace{+k_{+8}[E][P{:}I]}_{\substack{\text{Binding}\\ \text{of } P{:}I \text{ to } E}} - \underbrace{k_{-8}[E{:}P{:}I]}_{\substack{\text{Unbinding}\\ \text{of } P{:}I \text{ to } E}} \tag{16h}$$

$$\frac{d[P{:}I{:}E]}{dt} = \underbrace{k_{+5}[E][P{:}I]}_{\substack{\text{Binding}\\ \text{of } P{:}I \text{ to } E}} \underbrace{-k_{-5}[P{:}I{:}E]}_{\substack{\text{Unbinding}\\ \text{of } P{:}I \text{ from } E}} \underbrace{+k_{+7}[E{:}P{:}I]}_{\substack{\text{Transition of}\\ P{:}I{:}E \text{ to } E{:}P{:}I}} \underbrace{-k_{-7}[P{:}I{:}E]}_{\substack{\text{Transition of}\\ P{:}I{:}E \text{ to } E{:}P{:}I}}. \tag{16i}$$

Notice the differential equations corresponding to species that enter or exit the reaction zone (S,I, $P{:}I$, P) include a k_{flow} term. The equations for the two species entering the reaction zone from up-stream (S and I) also include their corresponding up-stream concentration ($[S_{up}]$ and $[I_{up}]$).

Since I am working with a nine-dimensional nonlinear system of ODEs, it

is extremely hard to find solutions analytically in practice. So, I solved the system of differential equations numerically using Mathlab's built-in function `ode23`, which is a single-step solver and implements the explicit Runge-Kutta method of third order[3, 27].

The initial concentrations for species entering the reaction zone are fixed to be $S_{up} = 170$nM (taken from [18]) and $I_{up} = 2.4$nM (taken from [24]), which are the physiological values used in experiments. The total amount of enzyme initially available in the reaction zone, denoted E_{Total}, is set to be 1.024nM (the highest enzyme value used for the static experiments considered in my study). All the other species' concentrations are zero initially. I used the same set of kinetic rates calculated in the previous section for the static model. The flow rates vary between 1e-3 $\leq k_{flow}(1/s) \leq$ 1e3 biologically (for more details see Appendix 3.4). I define $k_{flow} = 0$ as no flow, $k_{flow} =$ 1e-3 as low flow, $k_{flow} = 1$ as mid flow, and $k_{flow} =$ 1e3 as high flow.

2.3.3 Comparing the Significance of Different Mechanisms of TFPI

Reaction Number	Biochemical Reaction	*Indirect Binding* (IB)	*Direct Binding* (DB)	*Direct and Indirect Binding* (DB-IB)
1	$E + S \underset{k_{-1}}{\overset{k_1}{\rightleftharpoons}} E{:}S$	✓	✓	✓
2	$E{:}S \xrightarrow{k_2} E{:}P$	✓	✓	✓
3	$E + P \underset{k_{-3}}{\overset{k_3}{\rightleftharpoons}} E{:}P$	✓	✓	✓
4	$P + I \underset{k_{-4}}{\overset{k_4}{\rightleftharpoons}} P{:}I$	✓	$k_4 = k_{-4} = 0$	✓
5	$E + P{:}I \underset{k_{-5}}{\overset{k_5}{\rightleftharpoons}} P{:}I{:}E$	✓	$k_5 = k_{-5} = 0$	✓
6	$E{:}P + I \underset{k_{-6}}{\overset{k_6}{\rightleftharpoons}} E{:}P{:}I$	$k_6 = k_{-6} = 0$	✓	✓
7	$E{:}P{:}I \underset{k_{-7}}{\overset{k_7}{\rightleftharpoons}} P{:}I{:}E$	$k_7 = k_{-7} = 0$	✓	✓
8	$E + P{:}I \underset{k_{-8}}{\overset{k_8}{\rightleftharpoons}} E{:}P{:}I$	$k_8 = k_{-8} = 0$	$k_8 = k_{-8} = 0$	✓

Table 4: Mechanisms of TFPI Inhibition

To understand the role of TFPI in inhibiting TF:VIIa, I consider three different inhibition mechanisms based on the biochemical reactions: *Indirect Binding* (denoted IB), *Direct Binding* (denoted DB), and *Direct and Indirect Binding* (denoted DB-IB). As illustrated in Table 4, the inhibition through *Indirect Binding* involves reactions (1-5); the inhibition by *Direct Binding* consists of reactions (1-3 and 6-7); and the inhibition via *Direct and Indirect Binding* incorporate biochemical reactions (1-8). In order to compare the amount of inhibition happening across all these mechanisms, I define the inhibition of E,

denoted $E_{Inhibited}$, to be the concentration of enzyme that is bound and thus is unable to convert S to P. $E_{Inhibited}$ is quantified by summing the total concentration of E that is occupied by either P or P:I and is described mathematically as follows:

$$[E_{Inhibited}] = [E{:}P] + [E{:}P{:}I] + [P{:}I{:}E].$$

2.3.4 Results

All the results presented in this section focus on the total concentration of inhibited TF:VIIa ($[E_{Inhibited}]$) at steady-state to understand the long-term inhibition of E. The steady-state concentrations of $E_{Inhibited}$ were obtained by running the model simulation for a long time $t = 1e6(s)$. The first part of the results aims to determine the inhibition of TF:VIIa in the presence and absence of flow across different inhibition mechanisms, which include No TFPI and TFPI. The second part focuses on understanding how doubling or halving $K_{D,3}$ affects the overall inhibition of TF:VIIa (E) for varying flow rates across different mechanisms.

Inhibition of E in the Presence and Absence of Flow across different inhibition mechanisms

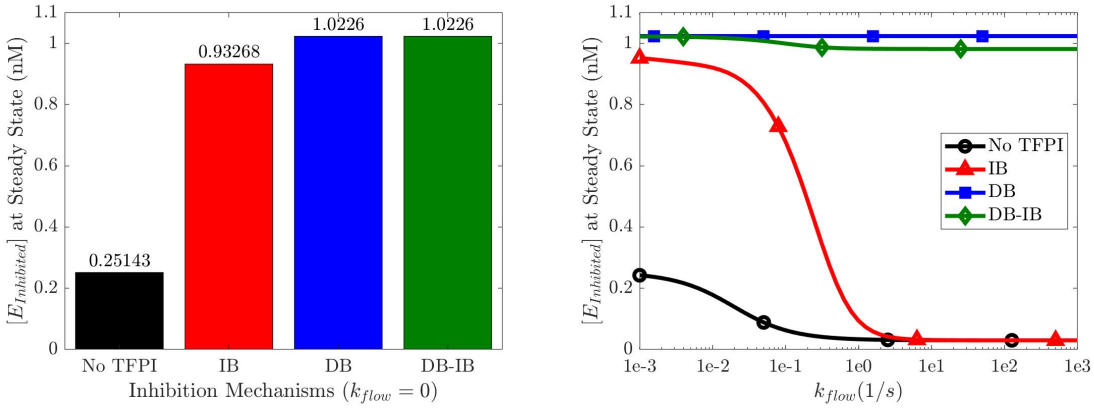

(a) No Flow **(b)** Varying Flow

Figure 7: The steady state concentration of $E_{inhibited}$ for (a) no flow ($k_{flow} = 0$) with fixed $[S] = 170$nM, $[E] = 10$nM, and $[I] = 2.4$nM; and (b) varying flow rates ($k_{flow} \neq 0$) with fixed $[E_{Total}] = 10$nM,$[S_{up}] = 170$nM, and $[I_{up}] = 2.4$nM in the absence of TFPI (black) and the presence of TFPI: with *Indirect Binding* (IB) mechanism (red), with *Direct Binding*(DB) mechanism (blue), and with *Direct and Indirect Binding (DB-IB)* mechanism (green).

Figure 7 represents the relationship between the inhibited concentration of TF:VIIa $[E_{Inhibited}]$ at steady state and: (7a) no flow ($k_{flow} = 0$) with fixed $[E] = 10$nM, $[S] = 170$nM, and $[I] = 2.4$nM; (7b) varying flow rates ($k_{flow} \neq 0$) for fixed $[E_{Total}] = 10$nM, $[S_{up}] = 170$nM, and $[I_{up}] = 2.4$nM in the absence of

TFPI (black) and in the presence of TFPI: with *Indirect Binding* mechanism (red), with *Direct Binding* mechanism (blue), with *Direct and Indirect Binding* mechanism (green). As depicted in subfigures (7a-7b), it can be observed that $[E_{inhibited}]$ is approximately the same for both no flow ($k_{flow} = 0$) and low flow (k_{flow} =1e-3) across all the different mechanisms. The detailed analysis of each inhibition mechanism is described below.

No TFPI (black): when there is no inhibitor in the system, the inhibition of E is only possible by the complex E:P. In this case, the concentration of $[E_{inhibited}]$ at steady state is approximately 0.25 nM for both no flow and low flow rates. It decreases gradually as k_{flow} varies from low to mid flow rates, and it flattens out for mid to high flow rates. The decrease in the $E_{inhibited}$ concentration is due to flow, which washes away free P from the reaction as it increases. This suggests that flow itself is both procoagulant and anticoagulant. On the one hand, flow promotes inhibition by bringing clotting factors to the injury site, but on the other hand, flow hinders inhibition by washing away free factor Xa (high flow).

Indirect Binding (red): With TFPI present in the system, the concentration of $E_{inhibited}$ via the *Indirect Binding* mechanism is four times stronger than when there is no TFPI in the system (black) for no flow and low flow rates as described in (7a-7b). For low to mid flow rates, $[E_{inhibited}]$ decreases gradually at first and then rapidly plunges to the same amount of inhibition as the case when there is no TFPI in the system. After that, it stays steady as flow varies between mid and high flow rates. The sudden decrease in inhibition level is due to the flow removing free P and P:I from the reaction zone and forbidding the latter's binding to free E fixed at the injury site.

Direct Binding (blue): The concentration of $E_{Inhibited}$ for the *Direct Binding* mechanism is flattened out approximately at E_{Total} across all flow rates as depicted in (7a-7b). In this case, there is a total inhibition of E because the flow does not have the ability to remove P from the reaction zone since I directly binds to P while the latter is bound to E, which is fixed at the injury site.

Direct and Indirect Binding (green): when both TFPI binding mechanisms are at play, $[E_{Inhibited}]$ is approximately at its maximum capacity (i.e. E_{Total}) for no flow and low flow. It slowly reduces by 5% for low to mid flow rates and stays steady as flow increases. The reduction in the inhibition is due to the presence of free P and P:I in the fluid, and the species are subject to being washed away by the flow.

Overall, it can be observed that the flow both helps and hinders the inhibition of E when there is no TFPI in the system. The presence of TFPI in the system does increase the concentrations of $E_{Inhibited}$ across all the mechanisms except for *Indirect Binding* at mid to high flow rates. It can also be observed that the *Indirect Binding* is the most sensitive to inhibition mechanism to flow. Both *Direct Binding* alone and *Direct and Indirect Binding* mechanisms are less sensitive to flow.

Total Inhibition of E in the Presence of Flow for varying $K_{D,3}$

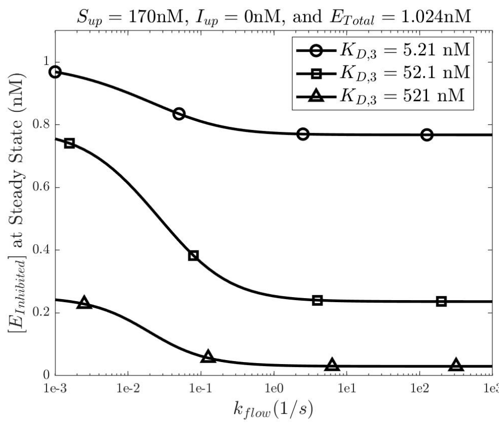

(a) No TFPI

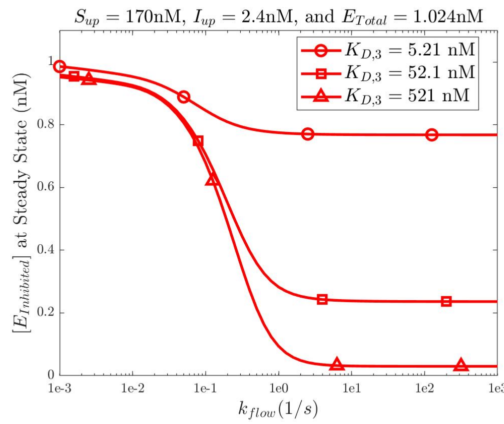

(b) *Indirect Binding* Mechanism

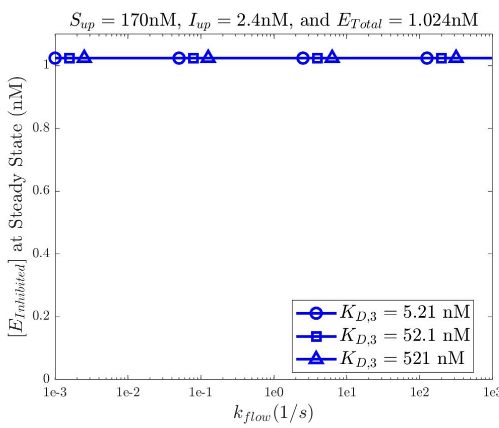

(c) *Direct Binding* Mechanism

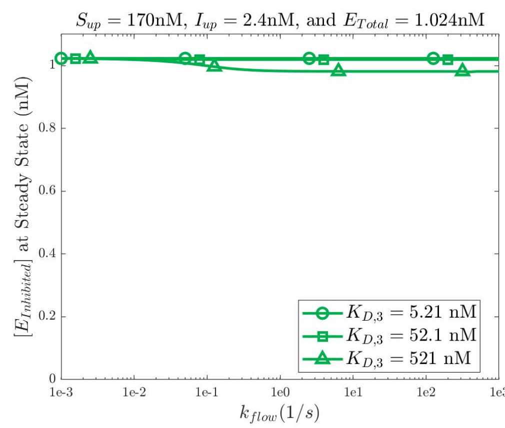

(d) *Direct and Indirect Binding* Mechanism

Figure 8: $E_{Inhibited}$ as k_{flow} increases under different $K_{D,3}$ (5.21nM (◯), 52.1nM, (□), and 521 nM (△) for different TFPI mechanisms: (a) No TFPI, (b) *Indirect Binding* Mechanism, (c)*Direct Binding* Mechanism, and (d)*Direct and Indirect Binding* Mechanism.

Next, I am interested in determining how varying $K_{D,3}$ affects $E_{Inhibited}$ across different mechanisms, and this relationship is described by Figure 8. Generally, a smaller value of $K_{D,3}$ indicates greater binding affinity between P & E and vice-versa. This can be seen when there is no TFPI in the system, decreasing $K_{D,3}$ increases inhibition levels as illustrated in Figure 8a due to product inhibition. For the TFPI *Indirect Binding* mechanism, I discover that $E_{Inhibited}$ varies slightly regardless of $K_{D,3}$ for low flow rates, but it is sensitive to $K_{D,3}$ values under higher flow rate. Again, the increase in the concentration of $E_{Inhibited}$ for mid to high flow as $K_{D,3}$ decreases is due to the strong product inhibition, suggesting that product inhibition itself and flow are stronger inhibitors than TFPI. These results are consistent with the results from the prior study by Fogelson et al. [10] about TFPI indirect binding. On the other

hand, the concentration of $E_{Inhibited}$ through TFPI *Direct Binding* mechanism is insensitive to $K_{D,3}$ across all flow rates (see Figure 8c) suggesting that TFPI itself is a stronger inhibitor than product inhibition or flow. For both *Direct and Indirect Binding* mechanisms, the concentration of $E_{Inhibited}$ is the same for $K_{D,3} = 5.21$ and $K_{D,3} = 52.1$, but it slightly decreases for a higher $K_{D,3}$ when flow rates are high (see Figure 8d). This also suggests that the presence of *Direct Binding* mechanism is important to understand the full role of TFPI.

2.4 Discussion and Conclusions

The main objective of my study was to develop a framework for TFPI mechanisms that aligns with well-established experimental data published by Baugh et al. [2]. To achieve this, I conducted a thorough mathematical analysis of the mechanisms of TFPI inhibition, specifically focusing on the scheme proposed in the same study (*Scheme II*). The purpose was to establish a set of kinetic rates that simultaneously fit the TFPI ODEs static model to the experimental data.

First, I employed constrained optimization to re-estimate the value of $K_{D,4}$ and utilized this updated value, along with known rates and relationships, to optimize the remaining kinetic rates. By employing constrained optimization, which enforces known values and relationships, I successfully identified a set of kinetic rates that fitted the TFPI ODEs static model across multiple time series data. The results obtained from the TFPI ODEs static model indicate that *Scheme II* has the potential to explain qualitatively all the experimental data and effectively describe the role of TFPI in inhibiting Xa formation in a static system. The fitting of the TFPI ODEs model is innovative because previous studies [2, 26] could not fit or sort the data correctly. The previous studies failed to fit the data because of the choice of kinetic rates. When I attempted to redo the fitting using the kinetic rate ranges Panteleev et al. [26] gave in their study, I had to set $k_{-6} = k_{+7} = k_{-7} = k_{-8} = 0$ to reproduce the identical results published in their studies. Moreover, they used the previously reported of $K_{D,4}$ from Baugh et al. [2]. The dissociation constants for all the other rates are identical or have the same order of magnitude.

In order to gain a deeper understanding of the system within a real physical context, I further investigated the two mechanisms in the presence of flow. Overall, the TFPI ODEs flow model findings highlight the significance of *Direct Binding* mechanism, where E directly binds P:I, in regulating the formation of P by I. Additionally, I quantified the level of inhibition by examining the concentrations of TF:VIIa bound to Xa or TFPI. The analysis led to the conclusion that *Direct Binding* mechanism exhibits the strongest inhibitory effect, which is further enhanced by the presence of flow. On the other hand, *Indirect Binding* mechanism is characterized as a weak inhibitor, and its effect is diminished by flow. The results for the *Indirect Binding* mechanism are consistent with the study by Fogleson et. al [10], in which it was concluded that TFPI has no inhibitory effect on TF exposure and flow itself is a more potent inhibitor.

For my results, It was also observed that the combined action of *Direct*

and Indirect Binding mechanism provides a higher level of inhibition compared to *Indirect Binding* mechanism alone, although it remains weaker than the inhibition achieved by *Direct Binding* mechanism due to the potential removal of the Xa:TFPI complex by the flow. In summary, the presence of *Direct Binding* mechanism is essential for regulating Xa and its inhibition by TFPI in the presence and absence of flow.

References

[1] Robert A. Alberty and Gordon G. Hammes. Application of the theory of diffusion-controlled reactions to enzyme kinetics. The Journal of Physical Chemistry, 62(2):154–159, 1958.

[2] Robert J. Baugh, George J. Broze, and Sriram Krishnaswamy. Regulation of extrinsic pathway factor Xa formation by tissue factor pathway inhibitor. Journal of Biological Chemistry, 273(8):4378–4386, 1998.

[3] P. Bogacki and L.F. Shampine. A 3(2) pair of runge - kutta formulas. Applied Mathematics Letters, 2(4):321–325, 1989.

[4] Alexei Botchkarev. Performance metrics (error measures) in machine learning regression, forecasting and prognostics: Properties and typology. 9 2018.

[5] Alan C. Burton. Relation of structure to function of the tissues of the wall of blood vessels. Physiological Reviews, 34(4):619–642, 1954. PMID: 13215088.

[6] Xia Cao, Sushila Maharjan, Ramla Ashfaq, Jane Shin, and Yu Shrike Zhang. Bioprinting of small-diameter blood vessels. Engineering, 7(6):832–844, 2021.

[7] Jeffrey A Cohlberg. Km as an apparent dissociation constant. Journal of Chemical Education, 56(8):512, 1979.

[8] Christopher M Danforth, Thomas Orfeo, Stephen J Everse, Kenneth G Mann, and Kathleen E Brummel. Defining the Boundaries of Normal Thrombin Generation : Investigations into Hemostasis. 7(2), 2012.

[9] E. Doutel, Francisco Galindo-Rosales, and Laura Campo-Deaño. Hemodynamics challenges for the navigation of medical microbots for the treatment of cvds. Materials, 14:7402, 12 2021.

[10] Aaron L. Fogelson and Nessy Tania. Coagulation under flow: The influence of flow-mediated transport on the initiation and inhibition of coagulation. Pathophysiology of Haemostasis and Thrombosis, 34(2-3):91–108, 2005.

[11] Z F Huang, T C Wun, and G J Broze. Kinetics of factor xa inhibition by tissue factor pathway inhibitor. Journal of Biological Chemistry, 268(36):26950–26955, 1993.

[12] The MathWorks Inc. fmincon, 2023.

[13] Ng Zhang Jin and Subash C.B. Gopinath. Potential blood clotting factors and anticoagulants. Biomedicine and Pharmacotherapy, 84:356–365, 12 2016.

[14] Kenneth A. Johnson and Roger S. Goody. The original michaelis constant: Translation of the 1913 michaelis–menten paper. Biochemistry, 50(39):8264–8269, 2011. PMID: 21888353.

[15] Andrew L. Kuharsky and Aaron L. Fogelson. Surface-mediated control of blood coagulation: The role of binding site densities and platelet deposition. Biophysical Journal, 80(3):1050–1074, 2001.

[16] Karin Leiderman and Aaron L. Fogelson. Grow with the flow: a spatial–temporal model of platelet deposition and blood coagulation under flow. Mathematical Medicine and Biology: A Journal of the IMA, 28(1):47–84, 05 2010.

[17] Genmin Lu, George J. Broze, and Sriram Krishnaswamy. Formation of factors IXa and Xa by the extrinsic pathway: Differential regulation by tissue factor pathway inhibitor and antithrombin III. Journal of Biological Chemistry, 279(17):17241–17249, 2004.

[18] Kenneth Mann, M Nesheim, William Church, P.E. Haley, and Sriram Krishnaswamy. Surface-dependent reactions of the vitamin k-dependent enzyme complexes. Blood, 76:1–16, 08 1990.

[19] Alejandro Marangoni. Enzyme Kinetics: A Modern Approach, pages 44 – 60. 03 2003.

[20] Susan A. Maroney, Randal J. Westrick, Audrey C. Cleuren, Nicholas D. Martinez, Amy E. Siebert, Mark Zogg, David Ginsburg, Hartmut Weiler, and Alan E. Mast. Tissue factor pathway inhibitor is required for cerebrovascular development in mice. Blood, 137(2):258–268, 01 2021.

[21] Franklin C. McLean. Application of the law of chemical equilibrium (law of mass action) to biological problems. Physiological Reviews, 18(4):495—-523, 1938.

[22] Jorge Nocedal and Stephen J. Wright. Numerical Optimization. Springer, New York, NY, USA, 2e edition, 2006.

[23] Brian V. Norledge, Ramona J. Petrovan, Wolfram Ruf, and Arthur J. Olson. The tissue factor/factor viia/factor xa complex: A model built by docking and site-directed mutagenesis. Proteins: Structure, 53, 2003.

[24] William F. Novotny, Susan G. Brown, Joseph P. Miletich, Daniel J. Rader, and George J. Broze. Plasma antigen levels of the lipoprotein-associated coagulation inhibitor in patient samples. Blood, 78(2):387–393, 1991.

[25] Andrea Orfanakis and Thomas DeLoughery. Patients with disorders of thrombosis and hemostasis. Medical Clinics of North America, 97:1161–1180, 11 2013.

[26] Mikhail A. Panteleev, Veronica I. Zarnitsina, and Fazoil I. Ataullakhanov. Tissue factor pathway inhibitor. European Journal of Biochemistry, 269(8):2016–2031, 2002.

[27] Lawrence F. Shampine and Mark W. Reichelt. The matlab ode suite. SIAM Journal on Scientific Computing, 18(1):1–22, 1997.

[28] Michael T. Stobb, Dougald M. Monroe, Karin Leiderman, and Suzanne S. Sindi. Assessing the impact of product inhibition in a chromogenic assay. Analytical Biochemistry, 580:62–71, 2019.

[29] Jeremy P Wood, Paul E R Ellery, Susan A Maroney, and Alan E Mast. Biology of tissue factor pathway inhibitor. 2014.

[30] M. E. Young, P. A. Carroad, and R. L. Bell. Estimation of diffusion coefficients of proteins. Biotechnology and Bioengineering, 22(5):947–955, 1980.

3 Appendix

3.1 Analysis of the Dissociation Constant for Inhibition of Factor Xa by TFPI

Consider the biochemical reaction that describes the inhibition of Xa by TFPI

$$Xa + TFPI \underset{k_{-4}}{\overset{k_{+4}}{\rightleftharpoons}} Xa : TFPI. \tag{17}$$

Experiment Description: The experiment consists in mixing initial concentrations of $Xa_0 = 0.1\ nM$ and $Xa_0 = 0.2\ nM$ with increasing concentration of TFPI and keeping track of the residual factor Xa concentration after a prolonged incubation in both cases.

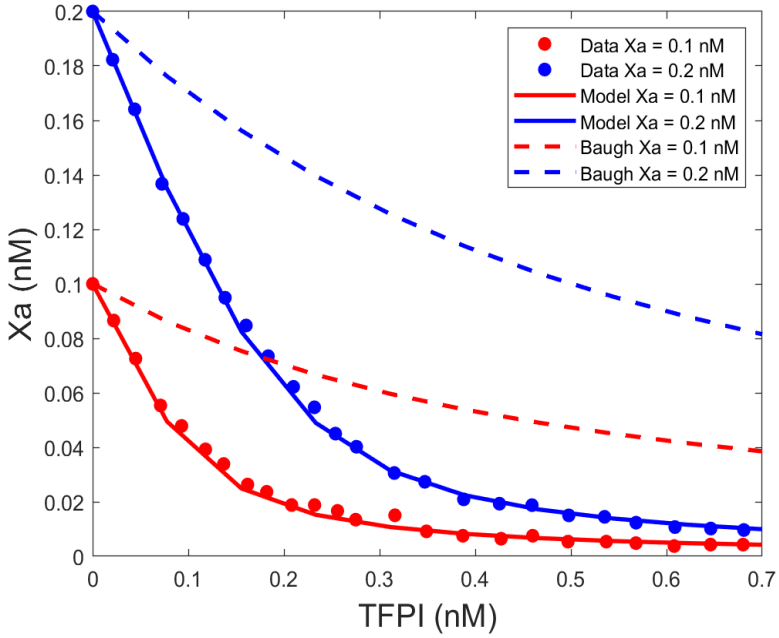

Figure 9: Inhibition of factor Xa by TFPI (left) The residual factor Xa as TFPI increases for initial concentrations of $Xa = 0.1\ nM$ (in red) and $Xa = 0.2\ nM$ (in blue) following prolonged incubation. The dashed line is model output for using kinetic rates k_{+4} and k_{-4} given by [2] and the solid line is the model fit to the data.

We extracted the two data sets of residual Xa concentrations with from figure 4 in the Baugh paper (extraction process is explained below) and plotted it along with the model output for Xa concentration called 'Baugh Xa' (dashed lines in Figure 9) for reaction 17 using the corresponding kinetic rates $k_{+4} = 0.9\ \mu M^{-1}s^{-1}$ and $k_{-4} = 3.6 \times 10^{-4} \cdot s^{-1}$ (taken from column 1 of table 1 from [2]). We found a huge difference between the model and the data outputs. After

a close analysis, we discovered that the reported kinetic rates for 17 in [2] are different by factor of 1/15 as compared to the kinetic rates found by fitting the data. This mean, that any k and k_{-4} that satisfy the equality

$$\frac{k_{+4}}{k_{-4}} = \frac{K_{D,4}}{15}$$

can fit the data to the model. However, we interesting in knowing what is the optimal $K_{D,4}$ that can fit the two experimental data sets effectively.

Steps to find the optimal value of dissociation constant for inhibition of Xa by TFPI

1. Solve the steady state in terms of [Xa] for reaction 17
2. find all the possible dissociation constant values using the steady state for [Xa] found in step 1 and data extracted in step 2.
3. find the optimal dissociation constant using constrained optimization.

Step 1 Using the Law of Mass Action, we can write the reaction 17 as a system of differential equations given below

$$\begin{aligned}
\frac{d[Xa]}{dt} &= -k_{+4}[XA][TFPI] + k_{-4}[Xa:TFPI] \\
\frac{d[TFPI]}{dt} &= -k_{+4}[Xa][TFPI] + k_{-4}[Xa:TFPI] \\
\frac{d[Xa:TFPI]}{dt} &= +k_{+4}[Xa][TFPI] - k_{-4}[Xa:TFPI]
\end{aligned}$$

We can set each differential equations equal to zero for finding the equilibrium points of the system and we get an equation of the form

$$k_{-4}[Xa:TFPI] = k_{+4}[Xa][TFPI].$$

Dividing both sides by k_{+4} gives us

$$\frac{k_{-4}}{k_{+4}}[Xa:TFPI] = [Xa][TFPI].$$

Let $K_{D,4} = \frac{k_{-4}}{k_{+4}}$ be the dissociation constant for the reaction (17), then

$$K_{D,4}[Xa:TFPI] = [Xa][TFPI].$$

Then, we can use the conservation laws

$$[Xa:TFPI] = [Xa_0] - [Xa] \text{ and } [TFPI] = [TFPI_0] - [Xa:TFPI]$$

in the above equation to get

$$[Xa]^2 + ([TFPI_0] - [Xa_0] + K_{D,4})[Xa] - K_{D,4}[xa_0] = 0.$$

Solving for $[Xa]$ gives two quadratic solution

$$[Xa_{1,2}] = \frac{-([TFPI_0] - [Xa_0] + K_{D,4}) \pm \sqrt{([TFPI_0] - [Xa_0] + K_{D,4})^2 + 4[Xa_0]K_{D,4}}}{2}.$$

Since we are dealing with biological concentration, we will only accept the positive solution. In other words,

$$[Xa] = \frac{-([TFPI_0] - [Xa_0] + K_{D,4}) + \sqrt{([TFPI_0] - [Xa_0] + K_{D,4})^2 + 4[Xa_0]K_{D,4}}}{2}. \quad (18)$$

Step 2 Next, we implemented a code that

1. computes Xa concentration using the equation 18 for each $K_{D,4}$ given by (k_{+4}, k_{-4}) pair, where $0.01 \leq k_{-4} \leq 1$ and $10^{-8} \leq k_{+4} \leq 0.4$.
2. calculates the corresponding relative error for each (k_{+4}, k_{-4}) pair using:

$$\epsilon = \sum_{i=1}^{2} \left(\sum_{j=1}^{12} \frac{(Y_{i,j} - D_{i,j})^2}{D_{i,j}^2} \right)^{\frac{1}{2}} \quad (19)$$

   where $Y_{i,j}$ and $D_{i,j}$ are the computed Xa concentration and the data respectively at i^{th} experimental curve and j^{th} time point.
3. plot the dissociation constants $K_{D,4}$ (see Figure 10a) and error propagation (see Figure 10b) by varying k_{+4} and k_{-4}. The navy blue line in the first plot gives us the possible values of $K_{D,4}$ associated to minimum error. The region in navy blue in the second plot tells us the possible interval of k_{+4} and k_{-4} where the error is minimum. This information is useful in our optimization step.

Step 3 We use matlab built in constrained optimization function "fmincon" to optimize the value of $K_{D,4}$. The upper and lower bounds of (k_{+4}, k_{-4}) were found based on the dark blue region in figure 10 left panel.

- k_{+4} must be positive because it is a biological parameter.
- k_{-4} can at most be 1 nM due to diffusion limit.

The optimal value of the Dissociation constant for inhibition of Xa by TFPI was found to be

$$K_{D,4} = 0.0263 \ nM.$$

using the error formula found in Step 2 part 2 as an objective function.

3.2 Extraction of the data:

For all the figures using data points, the data was extracted by uploading the figure from the original paper to an online webpage http://www.graphreader.com/. Individual data points from the graph were selected and the intervals of both axis were provided. This online tool returned back two data sets,one for the x-axis and the one for the y-axis.

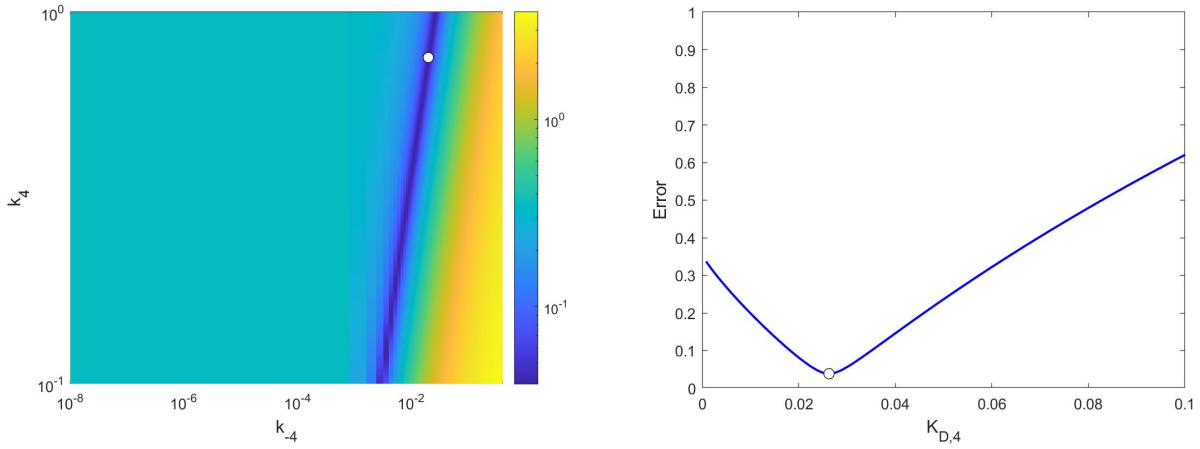

(a) **(b)**

Figure 10: The dissociation constant ($K_{D,4}$ (nM)) for each k_4 (s^{-1}) and k_{-4} $(nM^{-1}s^{-1})$ pair and the navy blue line represent $K_{D,4}$ nM associated to minimum error. (a) Error propagation on the log scale for residual Xa concentration for different $k_{4,off}$ and $k_{4,on}$ values. The navy blue region provides the optimal range for the kinetic rates associated to the $K_{D,4}$ with lowest error. The optimized $K_{D,4}$ is represented by the empty white circle present on the blue line. (b) Error propagation as dissociation constant $K_{D,4}$ increases.

3.2.1 *Experiment I Data:* Formation of P in Time for Various E Concentrations

3.2.2 *Experiment II Data: Formation of P in Time for Various P:I Concentrations*

Time	P(nM)							
	E = 0.032	E = 0.064	E = 0.128	E = 0.192	E = 0.256	E = 0.384	E = 0.512	E = 1.0
19	0.3044	1.0870	3.0435	5.6956	7.4783	13.6522	15.0435	20.434
34	0.8696	1.7826	4.8261	7.6956	9.4783	16.1304	19.6957	28.782
49	0.9565	2.2609	4.0869	8.4348	9.9130	14.4348	19.5217	30.826
64	0.9130	2.5217	5.2174	8.5217	9.4348	15.7391	18.6957	31.652
94	0.8696	1.9565	4.8696	8.2174	9.4348	16.6087	18.0870	34.739
124	0.7391	1.9565	4.6087	7.5652	9.1304	13.6957	17.0870	33.347
214	0.7391	1.7391	4.3044	7.2174	9.2609	14.8261	17.9130	34.173
304	0.5217	1.6957	4.6087	7.6087	10.0000	14.8696	18.4783	34.260
454	0.3044	1.4348	4.1739	7.5217	10.0869	16.3478	19.8261	33.695
604	0.0435	1.0870	4.7826	7.0435	10.0435	15.8261	18.0870	36.087
753	0.0869	1.0435	4.4783	8.0869	10.0435	16.5217	18.6087	32.217
900	0.2609	1.4348	5.1739	7.5652	9.1304	17.1304	20.4348	37.652

Table 5: Extracted data [2] for Xa concentration at time(s) (first column) for increasing concentrations of E(nM)(columns 2 through 9).

3.2.3 *Experiment III Data:* Inhibition of P by I

Time(s)	P (nM)			
	$P = 0$	$P = 0.25$	$P = 0.5$	$P = 1$
15	3.4400	2.4000	1.6000	1.1400
30	4.7400	3.0200	1.8000	1.2700
45	4.5900	3.0300	1.8700	1.2000
60	4.6300	2.8700	1.8700	1.2600
90	4.4500	2.9900	1.7500	1.2500
120	4.2200	2.7800	1.7500	1.2300
210	3.8800	2.4400	1.7600	1.2900
300	3.9600	2.3800	1.4000	1.0000
450	4.0100	2.3200	1.2600	1.4000
600	3.9400	2.3700	1.2800	1.1100
750	4.0300	2.3400	1.5900	0.8700
900	4.1500	2.6000	1.4400	1.2200

Table 6: Extracted data [2] for Xa concentration at time points (s) (first column) for increasing concentrations of P (nM)(columns 2 through 5).

3.3 Interior Point Method

Interior point methods represent a category of optimization algorithms used to solve linear and non-linear convex optimization problems. These iterative methods aim to maximize or minimize an objective function $f(\boldsymbol{x})$, which depends on decision variables $\boldsymbol{x}$ and is subject to constraints. These methods can handle both equality $C_E(\boldsymbol{x}) = 0$ and inequality constraints $C_I(\boldsymbol{x}) \geq 0$, which define the feasible region for the problem. Mathematically, the constrained minimization problem is formulated as follows

$$\min_{\boldsymbol{x}} f(\boldsymbol{x}) \ \textit{such that} \begin{cases} C_E(x) = 0 \\ C_I(x) \geq 0. \end{cases} \tag{20}$$

Let's rewrite the constrained optimization problem 20 in the standard form:

$$\min_{\boldsymbol{x},\boldsymbol{s}} f(\boldsymbol{x}) \ \textit{such that} \begin{cases} C_E(x) = 0. \\ C_I(x) - s = 0. \\ s \geq 0. \end{cases} \tag{21}$$

Note that we have converted the inequalities $C_I(x) \geq 0$ by introducing slack variables s. Moreover, let l denote the number of equality constraints $C_E(x)$ and let m denote the number of inequality constraints $C_I(x)$. To solve the problem 21, the interior point method uses a barrier approach, which consists in solving a sequence of approximate minimization problems. The approximate

$P = 0.1$ nM	
I(nM)	Rate($\Delta_{405} \times 10^{-3}/min$)
0	4.033
0.022	3.491
0.045	2.927
0.071	2.233
0.093	1.93
0.118	1.583
0.137	1.366
0.162	1.062
0.182	0.954
0.208	0.759
0.232	0.759
0.256	0.672
0.275	0.542
0.316	0.607
0.349	0.369
0.387	0.304
0.427	0.26
0.46	0.304
0.497	0.217
0.537	0.217
0.568	0.195
0.608	0.152
0.646	0.173
0.68	0.173

$P = 0.2$ nM	
I(nM)	Rate($\Delta_{405} \times 10^{-3}/min$)
0	7.7708
0.0209	7.0833
0.044	6.375
0.0725	5.3125
0.0945	4.8125
0.1176	4.2292
0.1385	3.6875
0.1604	3.2917
0.1835	2.8542
0.2099	2.4167
0.2319	2.125
0.2538	1.75
0.2758	1.5625
0.3154	1.1875
0.3473	1.0625
0.3879	0.8125
0.4253	0.75
0.4593	0.7292
0.4978	0.5833
0.5352	0.5625
0.5681	0.4792
0.6088	0.4167
0.6462	0.3958
0.6808	0.375

Table 7: Extracted data [2] for the residual factor Xa activity (second column) as the concentration of TFPI varies (1) for $P = 0.1$ nM (left) and $P = 0.2$ nM (right).

minimization problem can be formulated as follows:

$$\min_{\boldsymbol{x},\boldsymbol{s}} f_\mu(\boldsymbol{x},\boldsymbol{s}) = \min_{\boldsymbol{x},\boldsymbol{s}} f(\boldsymbol{x}) - \mu \sum_i^m \ln(s_i) \tag{22}$$
$$such\ that \begin{cases} C_E(x) = 0. \\ C_I(x) - s = 0. \end{cases}$$

where μ is a positive parameter, called barrier parameter, and $-\mu \sum_i^m \ln(s_i)$ is the barrier term also known as barrier function. The barrier term is used to enforce that the algorithm remains within the feasible region, defined by inequality constraints $C_I(x)$. Note that the inequality $s \geq 0$ is not included in problem 22 because the barrier term prevents s from getting too close to zero

(since $\ln(t) \to -\infty \; as \; t \to 0$), i.e. discouraging the algorithm from venturing outside the feasible region. As μ decreases with each iterate, the minimum of $f_\mu(\boldsymbol{x}, \boldsymbol{s})$ must get closer to the minimum of original function $f(x)$.

The interior point algorithm uses two main steps at each iteration to solve the approximate minimization problem. The first step (also known as Newton step) consists in solving KKT equations (for more details, check [22]) using a linear approximation. The second step consists of using a conjugate gradient step using trust region. As a standard procedure, the algorithm begins by trying to execute a direct step. If it encounters difficulty in doing so, it then attempts a conjugate gradient step.

3.4 Derivation of flow Rates

In their study, Fogelson et. al. defined the flow rate as "the rate at which flow brings a chemical[species] across the upstream (downstream)" and derived the following expression to calculate it

$$k_{flow} = \frac{3}{4}\left(\frac{V^2 D}{(RL)^2}\right)^{1/3}, \tag{23}$$

where V is the blood flow speed (midstream velocity of blood flow), D is the molecular diffusivity of a species, R is the radius of the vessel, and L is the length of the injury [15].

For my study, I determined the range of the flow rates (k_{flow}) based on the above equation (23). I fixed the diffusion coefficient to a previously reported literature value of $D = 5 \times 10^{-7} cm^2/s$ [30]. I kept the same assumptions for the injury length to be $L = 10\mu$M as assumed by Fogelson et al. [10]. I calculated the midstream velocities of the blood flow (V) as a function of radius (R) for varying flow rates. I determined the range of flow rates based on the previously reported radius and midstream blood flow velocities values for each vessel type, described in Table 8.

Vessel Type	Radius(μm) [5, 6]	Midstream Velocity ($\mu m/s$) [9]
Capillaries	(2e0,5e0)	(5e2,1e3)
Venules	(5e0,5e1)	(1e4,1e5)
Arteries	(5e1,5e3)	(1e5,5e5)
Veins	(5e1,5e4)	(3e5,1e5)

Table 8: Types of blood vessels with corresponding radius and midstream velocity.